heritage

MDPI

Article

Colors and Brilliance in the Wall Mosaic Assemblage of the Rotunda in Thessaloniki: A Physicochemical Investigation of the Glass Tesserae

Maria Kyranoudi [1,2,*], Lamprini Malletzidou [1,3,*], Eleni Pavlidou [1], George Vourlias [1] and Konstantinos Chrissafis [1]

[1] Laboratory of Advanced Materials and Devices, School of Physics, Faculty of Sciences, Aristotle University of Thessaloniki, GR-54124 Thessaloniki, Greece; elpavlid@auth.gr (E.P.); gvourlia@auth.gr (G.V.); hrisafis@physics.auth.gr (K.C.)
[2] Hellenic Ministry of Culture, Ephorate of Antiquities of Thessaloniki City, Heptapyrgion, P.O. Box 18432, GR-54003 Thessaloniki, Greece
[3] Laboratory of Archaeometry and Physicochemical Measurements, Athena—Research and Innovation Center in Information, Communication and Knowledge Technologies, Kimmeria University Campus, P.O. Box 159, GR-67100 Xanthi, Greece
* Correspondence: mkiranoudi@culture.gr (M.K.); l.malletzidou@athenarc.gr (L.M.)

Abstract

The Rotunda in Thessaloniki, Greece, preserves in its interior a magnificent wall mosaic assemblage of unique inspiration and beauty. Thirty-six (36) glass tesserae, blue, green, yellow, brown, black, gold and silver in color, were examined for the first time via UV-Vis reflectance spectroscopy, scanning electron microscopy with energy dispersive spectroscopy (SEM-EDS) and X-ray diffraction (XRD) analysis, in order to investigate the base glass composition, and their technological and morphological features. Despite the heterogeneity observed in the glass composition, the results indicated similarities with other Early Christian and Byzantine wall mosaics in the use of colorants, opacifiers and decolorizers. Cobalt, copper, iron and manganese along with lead and tin compounds are responsible for the blue, green, yellow, brown and black colors. Tin-based opacifiers and bone ash contribute to the glass opacity. The use of different glass recipes and opacifiers in the Rotunda's assemblage reflects the transition from the Roman glass tradition to the Byzantine glass production of the fourth and the fifth century in the eastern Mediterranean.

Keywords: Rotunda; glass; tesserae; mosaics; XRD; SEM-EDS; UV-Vis

check for updates

Academic Editors: Lucia Burgio and Silvano Mignardi

Received: 6 July 2025
Revised: 1 September 2025
Accepted: 17 September 2025
Published: 19 September 2025

Citation: Kyranoudi, M.; Malletzidou, L.; Pavlidou, E.; Vourlias, G.; Chrissafis, K. Colors and Brilliance in the Wall Mosaic Assemblage of the Rotunda in Thessaloniki: A Physicochemical Investigation of the Glass Tesserae. *Heritage* **2025**, *8*, 393. https://doi.org/10.3390/heritage8090393

Copyright: © 2025 by the authors. Licensee MDPI, Basel, Switzerland. This article is an open access article distributed under the terms and conditions of the Creative Commons Attribution (CC BY) license (https://creativecommons.org/licenses/by/4.0/).

1. Introduction

During the Byzantine Era, Thessaloniki was a significant center of wall mosaic art. Situated between Italy and the Middle East, both of which have provided significant collections of wall mosaics that have been well studied during the last decades, the city of Thessaloniki represents an interesting link between these two regions of different glass traditions [1,2]. A fine collection of early Christian and Byzantine wall mosaic decorations is preserved in situ at six monuments within the city, inscribed on the UNESCO World Heritage List, among which the Rotunda possesses a central place [3].

The Rotunda is a late antique domed building, erected in close vicinity to the triumphal arch of Galerius and the adjacent palace complex of Thessaloniki. Different theories have been proposed about its founder and about the initial use of the original

building [4–9]. Recent research attributes the Rotunda to Constantine I (305–337). The monument was erected to be his mausoleum and was converted into a Christian church after his death [10–13]. Parts of a magnificent wall mosaic ensemble are preserved in its interior, recognized as a masterpiece of Early Byzantine mosaic art. For the execution of this impressive mosaic composition, a wide range of colored and metal leaf glass tesserae along with stone tesserae have been used, contributing under the reflected sunlight to the beauty and glory of the monument's interior. Although the Rotunda's mosaics have intrigued scholars for decades both for their iconographic interpretation and their connection to the original building, the materials used for their manufacture had never been previously investigated in a systematic manner. In 2016 a scientific investigation of the monument's decoration was performed, which involved a multi methodological approach of the so called "S. Rosi" wall painting preserved on the eastern part of the dome [14], along with a non-invasive, in situ, color and X-ray fluorescence (XRF) examination of the mosaic tesserae. This examination of the wall mosaics reported some preliminary considerations about the chemical composition of the glass tesserae [15]. Intending to upgrade this initial study with a systematic investigation, additional analytical methods were applied to a group of thirty-six (36) individual tesserae, representative of the available colors, all having been found detached during conservation programs executed by the Hellenic Ministry of Culture on the Rotunda's mosaics in the past decades.

2. The Mosaic Decoration

The mosaic decoration of the monument's interior was developed in three concentric zones: on the dome (Figure 1a), on the lunettes of the dome base and on the arches of the eight niches of the ground floor level. The best preserved, lower zone of the dome is divided by vertical, vegetal motifs into eight panels (seven preserved nowadays) which depict male figures (Figure 1b,c), in a prayer position standing in front of elaborate architectural facades, accompanied by inscriptions. In the middle, poorly preserved zone fragments of sandaled feet and clothing on a green ground are observed, which correspond to about thirty-six male figures in a circular arrangement. On the top register of the mosaic composition, four angels held a medallion (Figure 1a) on which only the preparatory sketch on the brick substrate is preserved, depicting a male figure coming in glory [6,16]. Besides the dome, three of the eight niches of the ground floor level and four of the lunettes of the dome base preserve mosaic decoration on their vaults. The decoration is aniconic, with decorative motifs well known from the iconography of Roman and early Byzantine art of wall paintings and mosaics [17]. Different interpretations and dates have been suggested for the mosaics connecting them either with the original building (first half of the 4th c.) or with its conversion into a Christian church (4th–6th c.) [6,7,11,12,17]. The constructional and iconographic differences in the mosaic decoration on the vault of the southern niche of the ground floor level attribute this part of the decoration to a different, later chronological phase [12].

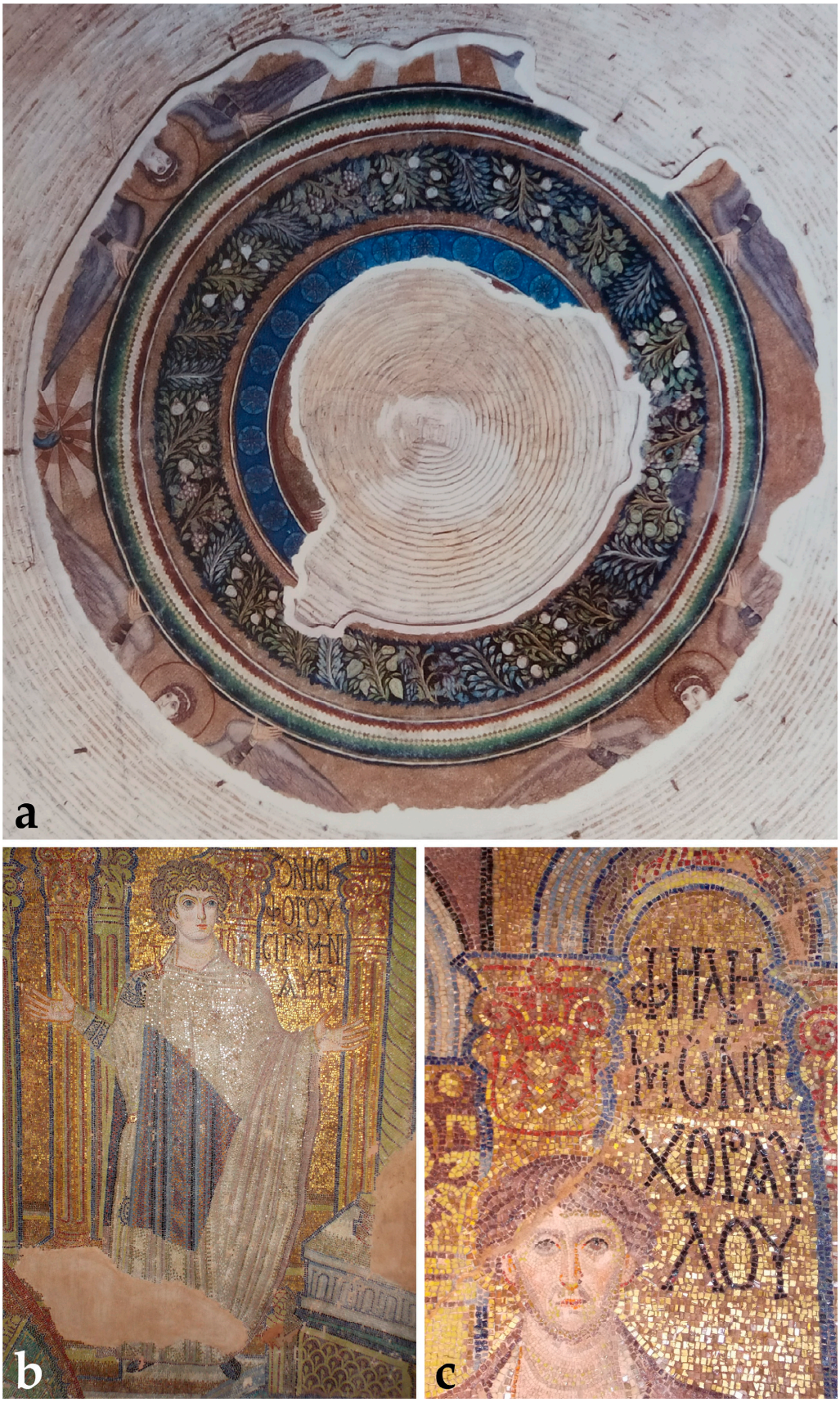


Figure 1. Representative preserved mosaic decoration of Rotunda: (**a**) The upper part of the dome decoration; (**b**,**c**) details from the zone of the male figures (photographic archives of the Ephorate of Antiquities of Thessaloniki City).

3. Materials and Methods

The thirty-six (36) tesserae under study were classified, macroscopically, into eleven (11) chromatic groups (light blue, blue, dark blue, light green, green, dark green, yellow, brown, black, gold leaf and silver leaf). For a more accurate color classification, the Munsell rock color chart [18] was used, under daylight, taking into account the restrictions that different parameters, such as thickness and light source, impose to the perception of color to the naked eye [19].

Preliminary examination of the tesserae was performed via optical microscopy (OM) with a DMS 300 stereomicroscope (Leica Microsystems GmbH, Wetzlar, Germany) equipped with a HD monitor for determining their morphological and structural features. Sample preparation, for the applied analytical methods, involved removing the weathered surface [20] from one side of each tessera by mechanical polishing using silicon carbide papers of grades up to 2000 grid. This preparation was chosen over resin embedding for handling, to maximize the information obtained from the inhomogeneous glass matrix and to minimize sample destruction. Samples R.B.L.3, R.B.D.3 and R.G.L.1 were excluded from the polishing procedure due to their brittleness. For the gold and silver leaf tesserae, a cross section, indicative of their "sandwich" arrangement including top glass or *cartellina*, metal leaf and base or support glass [21], was chosen for preparation, except for sample R.GO.2c which preserves only *cartellina* and gold leaf traces and was excluded from the preparation procedure too. The other gold tesserae have been undertaken double grid preparation for better removal of the weathered layers.

UV-Vis reflectance spectroscopy was applied to the semi-opaque colored samples (excluding the metal leaf tesserae due to the multiple layers) with a UV-Vis spectrometer, model Lambda 18 (PerkinElmer, Inc., Shelton, CT, USA) equipped with an integrating sphere. A tungsten and a deuterium illumination source were employed. Color coordinates were determined on the polished surfaces of the tesserae using barium sulfate as a reference. The results were expressed in the Commission Internationale de l'Eclairage (CIE) L*a*b* color space by using FR monitor v3.4 program (ThetaMetrisis S.A., Athens, Greece). Diffuse reflectance spectra were recorded in the wavelength range between 200 and 800 nm.

The morphology and the elemental analysis of each sample were investigated by means of scanning electron microscopy with an attached energy dispersive spectrometer (SEM-EDS). The polished sides of the samples—carbon coated—were analyzed with a JMS-840A electron microscope (JEOL Ltd., Akishima, Tokyo, Japan), equipped with an Oxford detector (Oxford Instruments plc, Abingdon, Oxfordshire, UK), model ISIS 300. The measurements were performed in low vacuum mode (20 kV accelerating voltage, 1 mA probe current and 15–20 mm working distance). SEM images were taken by collecting the backscattered electron signal (BSE). Averages of three surface EDS measurements per colored sample were calculated including inclusions and crystal phases, along with separate point measurements on inclusions, when detected, and the glass matrix. EDS measurements on metal leaf tesserae were taken separately on the base glass, *cartellina* and metal leaf. For sample R.GO.1, two final measurements on the base glass were taken because of the two different glass matrices detected. In total, forty-three (43) final measurements on the thirty-six (36) tesserae have been evaluated in EDS tables and diagrams. Eighteen (18) elements were calculated, expressed in weight per cent (wt%) of their most stable oxides (except for Cl). Instrument calibration was performed using standards of pure elements, oxides and minerals of known composition (standard 1773 Micro-Analysis Consultants Ltd., St. Ives, Cambridgeshire, UK). Accuracy and precision were verified daily using the same standards.

Phase identification of inclusions or crystalline phases was performed directly on the whole, polished samples by X-ray diffraction (XRD) analysis, using a two-cycle Rigaku Ultima^{+} X-ray diffractometer (40 kV/30 mA, CuKα radiation, in Bragg–Brentano geometry) (Rigaku Corporation, Akishima, Tokyo, Japan). The XRD patterns were collected from 5° to 60° angle 2-Theta, with a 0.02° step and a count of 4 s. The metal leaf samples were excluded from the XRD analysis in compliance with the permit provided by the Hellenic Ministry of Culture. The collected XRD patterns were identified with Powder Diffraction Files (PDF) of the International Centre for Diffraction Data (ICDD), formerly the Joint Committee on Powder Diffraction Standards (JCPDS) (release 2003).

4. Results and Discussion

The color classification after Munsell separated the color tesserae (excluding metal leaf groups) into thirteen (13) subgroups as listed in Table 1. The UV-Vis reflectance spectroscopy results for the colored samples were evaluated in the CIE L*a*b* color space (Table 1, Figure 2). Color presents three values, L* for perceptual lightness, a* (-a*) and b* (-b*), that make up the four unique colors of human vision: red, green, blue and yellow [22,23]. The classification after Munsell is generally in accordance with the sample distribution in CIE L*a*b* color space. Brown, black and dark blue are the most homogeneous color subgroups, while the other color categories are distributed in the space between yellow, green and blue, occupying separate areas. Although the two general categories of blue and green are distinguished from each other, their different hue subgroups are rather dispersed, in contrast with the macroscopic grouping. Furthermore, black tesserae are placed in the space between yellow and green, despite their seemingly black color, to the naked eye. Black does not exist as a color in CIE L*a*b* color space, but it represents the bottom of the luminosity scale (L = 0) [24].

Table 1. Encoding, optical images and color grouping of Rotunda's samples.

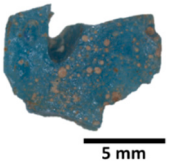
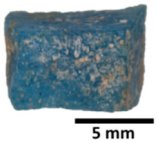
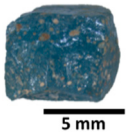
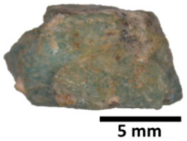
Sample Code	Chromatic Group (Macroscopic Classification)	Sample Photo	Color After Munsell	L*	a*	b*
R.B.L.1	Light blue Semi-opaque		5B 5/6 Moderate Blue	44.27	−14.25	−3.72
R.B.L.2	Light blue Semi-opaque		5B 5/6 Moderate Blue	4.37	−14.26	−8.06
R.B.L.5	Light blue Semi-opaque		5B 5/6 Moderate Blue	41.20	−14.67	−4.51
R.B.L.3	Light blue Semi-opaque		5BG 7/2 Pale Blue Green	71.26	−3.79	−0.75
R.B.L.4	Light blue Semi-opaque		5BG 7/2 Pale Blue Green	54.08	−8.15	4.16

Table 1. *Cont.*

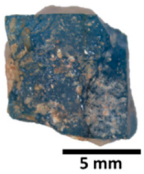
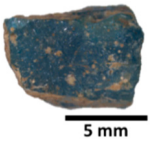
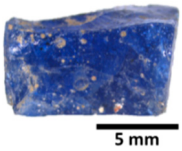
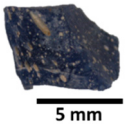
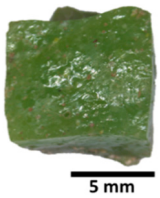
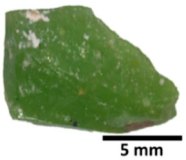
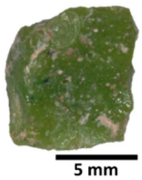
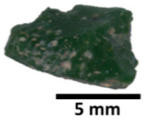
Sample Code	Chromatic Group (Macroscopic Classification)	Sample Photo	Color After Munsell	L*	a*	b*
R.B.M.1	Blue Semi-opaque		5B 5/6 Moderate Blue	24.32	−13.37	14.96
R.B.M.2	Blue Semi-opaque		5B 5/6 Moderate Blue	33.58	−4.95	−3.61
R.B.M.3	Blue Semi-opaque		5B 5/6 Moderate Blue	35.56	−11.5	−2.92
R.B.D.1	Dark blue Semi-opaque		5PB 3/2 Dusky Blue	20.90	−0.09	−7.15
R.B.D.2	Dark blue Semi-opaque		5PB 3/2 Dusky Blue	36.91	−1.08	−7.57
R.B.D.3	Dark blue Semi-opaque		5PB 3/2 Dusky Blue	34.90	0.75	−8.29
R.G.L.1	Light green Semi-opaque		10GY 6/4 Moderate Yellowish Green	49.33	−21.13	21.74
R.G.L.2	Light green Semi-opaque		10GY 6/4 Moderate Yellowish Green	27.17	−16.07	10.41
R.G.L.3	Light green Semi-opaque		10GY 6/4 Moderate Yellowish Green	46.10	−16.56	15.71
R.G.M.1	Green Semi-opaque		5G 5/6 Moderate Green	49.33	−12.51	7.88
R.G.M.2	Green Semi-opaque		5G 5/6 Moderate Green	28.98	−11.89	1.61

Table 1. *Cont.*

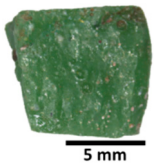
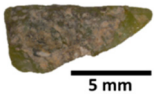
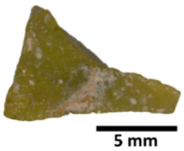
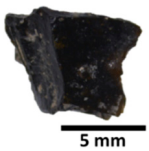
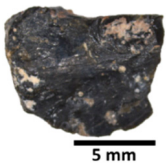
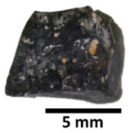
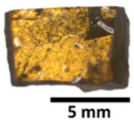
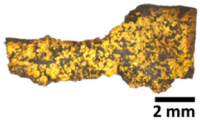
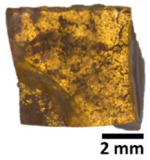
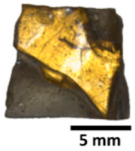
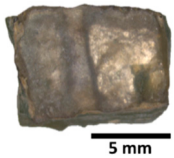
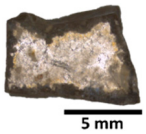
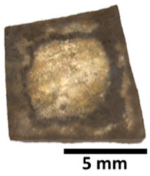
Sample Code	Chromatic Group (Macroscopic Classification)	Sample Photo	Color After Munsell	L*	a*	b*
R.G.M.3	Green Semi-opaque		5G 5/6 Moderate Green	42.87	−21.6	12.75
R.G.D.1	Dark green Semi-opaque		5BG 4/6 Moderate Blue Green	36.98	−16.71	7.52
R.G.D.2	Dark green Semi-opaque		5BG 4/6 Moderate Blue Green	37.95	−16.49	8.49
R.G.D.3	Dark green Semi-opaque		5BG 4/6 Moderate Blue Green	36.98	−9.84	7.58
R.Y.1	Yellow Semi-opaque		5GY 7/4 Moderate Yellow Green	56.46	−7.74	31.99
R.Y.3	Yellow Semi-opaque		5GY 7/4 Moderate Yellow Green	57.53	−5.68	17.31
R.Y.2	Yellow Semi-opaque		10Y 6/6 Dark Greenish Yellow	53.26	−3.07	17.79
R.BR.1	Brown Opaque		5R 2/2 Blackish Red	22.86	8.12	16.14
R.BR.2	Brown Opaque		5R 3/4 Dusky Red	29.65	9.34	13.05
R.BR.3	Brown Opaque		5R 4/6 Moderate Red	31.54	16.99	16.81
R.BL.1	Black Opaque		N2 Grayish Black	15.91	−2.87	13.02

Table 1. *Cont.*

Sample Code	Chromatic Group (Macroscopic Classification)	Sample Photo	Color After Munsell	L*	a*	b*
R.BL.3	Black Opaque		N2 Grayish Black	21.06	−2.69	8.45
R.BL.2	Black Opaque		N1 Black	25.35	−2.67	6.81
R.GO.1	Gold leaf Transparent yellowish/greenish					
R.GO.2	Gold leaf Transparent (only *cartellina*)					
R.GO.3	Gold leaf Transparent yellowish					
R.GO.4	Gold leaf Transparent yellowish/greenish					
R.S.1	Silver leaf Transparent yellowish/greenish					
R.S.2	Silver leaf Transparent yellowish					
R.S.3	Silver leaf Transparent yellowish					

SEM-EDS and XRD results are presented and discussed in the following, for the sum of the samples and per color group as classified with the naked eye, regarding light blue, blue, dark blue as one general group, and light green, green, dark green as a second general group. It should be mentioned that the samples present a continuous XRD pattern, characteristic of the amorphous glass base, disrupted with peaks when crystalline phases were present.

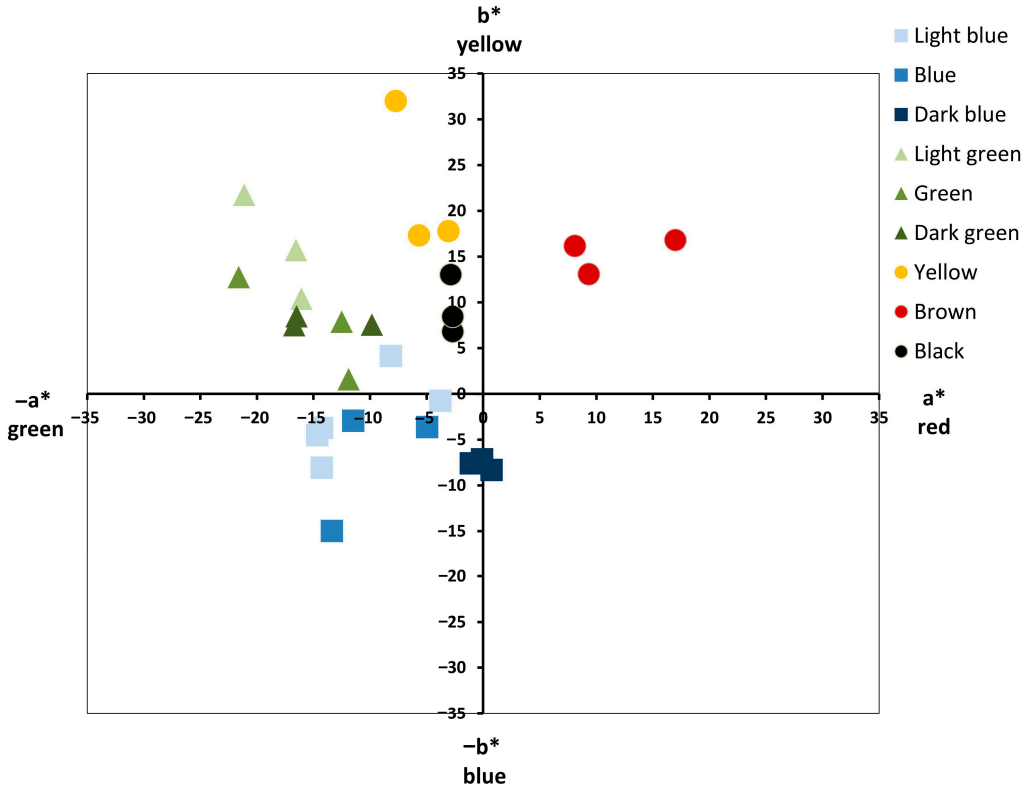


Figure 2. Chromatic coordinates of Rotunda's samples in CIE L*a*b* color space.

4.1. Base Glass Composition

Glass composition, as presented in Tables 2–4, was evaluated including oxides attributed to colorants, opacifiers and decolorizers, taking into account the difficulty in distinguishing between the contribution of the impurities found in base glass raw materials and the colorants' contribution.

The Rotunda's tesserae belong to the common type of soda–lime–silica glass. Silica is the main network former (average 54.08% for colored samples and 60.07% for metal leaf samples), soda is the main fluxing agent (average 15.25% for colored samples and 17.11% for metal leaf samples) and lime is the main stabilizer (average 10.41% for colored samples and 9.55% for metal leaf samples) (Table 4). Regarding the soda content, some samples (R.B.L.3, R.B.D.3, R.G.L.1, R.G.D.2, R.Y.2 and R.GO.2c) exhibit extremely low levels, varying from 2% to 6.93%. Low concentrations of soda have been mentioned in high potassium glass tesserae of Florence Baptistery [25], while they present much higher levels of potassium. Several researchers attribute similar low soda levels to glass corrosion, which causes leaching of alkalis in humid environment [20,26–31], or to the use of glass waste [32]. In the case of the Rotunda, samples R.B.L.3, R.B.D.3 and R.G.L.1 present a deteriorated surface, which explains the alkali depletion, and along with sample R.GO.2c were excluded from the preliminary polishing procedure. Traces of weathered glass on samples R.GO.2c, R.G.D.2 and R.Y.2 explain the measured similar low soda contents. These samples have been regarded as outliers and were excluded from the min, max and average EDS values (Table 4). In the rest of the colored and metal leaf tesserae, the soda content varies from 9.56% to 24.35% with an average of 16.00%.

Table 2. EDS elemental analysis of the Rotunda's colored tesserae (wt%). The averages of three surface measurements are presented (bdl: below detection limit).

Sample Code	Sample Color	Na_2O	MgO	Al_2O_3	SiO_2	P_2O_5	SO_3	Cl	K_2O	CaO	TiO_2	MnO	Fe_2O_3	CoO	CuO	ZnO	SnO_2	Sb_2O_3	PbO
R.B.L.1	Light blue	13.59	0.51	2.67	57.62	0.96	bdl	1.84	2.37	13.17	bdl	0.06	0.69	0.20	1.14	0.47	2.13	2.58	bdl
R.B.L.2	Light blue	11.92	0.54	1.30	62.37	0.47	0.74	3.87	2.02	11.14	0.38	0.12	0.73	bdl	1.51	bdl	1.17	1.73	bdl
R.B.L.3 *	Light blue	5.55	0.65	1.23	57.20	bdl	bdl	bdl	4.24	16.76	0.08	bdl	bdl	2.42	2.90	1.86	4.35	2.74	bdl
R.B.L.4	Light blue	16.39	0.81	1.84	56.73	bdl	0.42	4.21	1.36	13.90	bdl	0.33	0.86	bdl	0.07	bdl	1.27	1.57	0.25
R.B.L.5	Light blue	15.23	0.28	2.44	60.85	0.42	0.03	2.57	1.66	11.51	0.10	0.03	0.04	0.19	0.24	bdl	1.16	3.25	bdl
R.B.M.1	Blue	15.27	0.84	2.42	59.59	0.04	0.18	2.28	1.86	11.13	bdl	bdl	0.54	0.06	2.33	0.72	1.30	1.05	0.41
R.B.M.2	Blue	15.99	0.61	2.61	61.00	bdl	0.12	2.40	1.67	11.77	0.16	bdl	0.75	bdl	1.00	0.08	0.45	1.12	0.28
R.B.M.3	Blue	17.37	0.37	1.04	62.94	0.29	0.55	3.53	0.98	9.12	bdl	bdl	0.26	0.08	0.64	bdl	0.54	2.30	bdl
R.B.D.1	Dark blue	11.86	0.79	1.90	45.15	0.09	0.20	2.89	2.03	11.44	0.24	0.44	2.76	0.10	1.77	bdl	5.93	0.68	11.72
R.B.D.2	Dark blue	18.17	1.00	1.99	57.76	0.49	0.36	1.89	1.05	10.11	bdl	1.74	2.14	0.30	0.56	0.44	0.42	0.28	1.31
R.B.D.3 *	Dark blue	2.90	7.07	1.28	64.52	0.29	0.67	1.62	2.13	9.46	0.19	0.78	1.84	bdl	1.96	2.48	0.90	1.93	bdl
R.G.L.1 *	Light green	4.72	0.62	2.75	53.26	1.05	bdl	1.37	2.02	8.82	bdl	bdl	0.13	bdl	1.17	2.07	3.73	0.65	17.65
R.G.L.2	Light green	15.59	0.35	2.06	49.91	0.26	bdl	2.22	0.67	8.13	0.19	0.31	0.61	bdl	bdl	bdl	2.84	4.40	12.47
R.G.L.3	Light green	15.86	0.82	2.37	49.31	0.47	0.35	2.02	0.92	8.08	bdl	0.14	0.14	bdl	0.57	0.11	1.42	1.43	16.00
R.G.M.1	Green	15.83	0.37	2.47	50.63	bdl	bdl	1.88	1.64	7.23	bdl	0.12	bdl	bdl	1.37	bdl	2.54	0.36	15.58
R.G.M.2	Green	13.91	0.94	2.25	51.59	bdl	0.25	bdl	1.45	8.57	0.14	0.18	0.73	0.11	1.62	0.12	2.17	0.39	15.59
R.G.M.3	Green	15.46	0.27	2.26	53.16	bdl	bdl	2.38	0.75	9.55	0.30	bdl	0.34	bdl	0.62	0.09	0.12	0.52	14.18
R.G.D.1	Dark green	11.16	0.69	2.89	47.91	bdl	0.17	1.10	0.57	8.22	0.08	1.21	bdl	1.01	2.46	1.25	2.24	2.56	16.47
R.G.D.2 *	Dark green	6.93	0.43	1.83	49.32	0.14	bdl	2.92	2.20	13.49	0.21	1.04	0.96	bdl	0.13	bdl	1.02	0.80	18.59
R.G.D.3	Dark green	17.42	1.01	1.29	49.85	bdl	0.58	1.88	0.40	8.60	0.37	0.14	1.79	bdl	2.64	0.33	1.15	0.55	12.00
R.Y.1	Yellow	19.02	0.63	2.06	62.08	0.38	bdl	1.55	1.59	7.64	0.16	0.08	0.49	0.16	0.74	0.40	0.45	0.63	1.96
R.Y.2 *	Yellow	2.00	0.99	2.54	58.38	bdl	bdl	2.51	1.90	10.99	bdl	bdl	1.73	bdl	bdl	0.79	1.91	3.12	13.16
R.Y.3	Yellow	17.28	0.42	2.63	50.26	0.62	1.11	2.33	2.13	6.73	0.37	0.02	0.63	0.02	0.31	bdl	3.89	1.25	10.00
R.BR.1	Brown	13.45	1.00	2.33	54.82	0.86	0.05	3.00	2.82	11.81	0.26	bdl	3.97	0.19	1.33	bdl	1.77	0.35	1.99
R.BR.2	Brown	12.03	0.95	1.99	45.63	0.34	0.15	2.59	2.01	11.22	0.23	0.40	2.69	bdl	1.84	bdl	5.57	1.06	11.32
R.BR.3	Brown	9.56	0.54	1.89	46.66	0.47	0.31	2.89	2.35	14.44	0.07	0.27	3.54	bdl	1.54	bdl	4.32	1.93	9.22

Table 2. *Cont.*

Sample Code	Sample Color	Na_2O	MgO	Al_2O_3	SiO_2	P_2O_5	SO_3	Cl	K_2O	CaO	TiO_2	MnO	Fe_2O_3	CoO	CuO	ZnO	SnO_2	Sb_2O_3	PbO
R.BL.1	Black	10.95	0.49	1.54	56.63	0.11	0.49	4.64	1.85	17.92	0.26	0.55	1.13	0.05	0.10	bdl	1.47	1.75	0.07
R.BL.2	Black	24.35	1.84	2.72	57.81	0.45	bdl	1.59	0.74	5.53	0.04	1.35	2.96	0.16	0.12	0.15	bdl	0.19	bdl
R.BL.3	Black	22.06	1.94	1.65	55.77	0.38	0.99	3.19	1.46	10.10	0.18	0.16	0.37	0.03	0.54	bdl	0.54	0.52	0.14

* Sample excluded from average values of Table 4.

Table 3. EDS elemental analysis of the Rotunda's metal leaf tesserae (wt%). The averages of three surface measurements are presented) (s = supporting glass, a–b = different supporting glass in the same tessera, c = *cartellina*, bdl: below detection limit).

Sample Code	Sample color	Na_2O	MgO	Al_2O_3	SiO_2	P_2O_5	SO_3	Cl	K_2O	CaO	TiO_2	MnO	Fe_2O_3	CoO	CuO	ZnO	SnO_2	Sb_2O_3	PbO
R.GO.1sa	Yellowish naturally colored/Golden leaf	19.44	0.77	1.65	58.09	0.32	0.35	2.76	0.87	7.26	0.67	0.62	0.47	0.06	bdl	1.18	1.54	3.28	0.69
R.GO.1sb	Greenish naturally colored/Golden leaf	20.32	1.01	2.13	57.76	0.36	bdl	2.45	1.15	7.73	0.30	1.90	0.62	bdl	bdl	bdl	1.42	2.82	bdl
R.GO.1c	Yellowish naturally colored/Golden leaf	19.14	0.53	1.89	59.45	0.31	0.47	2.32	1.18	7.48	0.19	1.50	0.90	0.03	0.06	bdl	1.81	2.73	bdl
R.GO.2c *	Colorless/Golden leaf	4.09	0.94	2.27	70.58	bdl	0.56	2.26	4.41	12.20	bdl	0.73	1.06	bdl	bdl	bdl	0.65	bdl	0.26
R.GO.3s	Yellowish naturally colored/Golden leaf	20.56	0.52	2.00	56.87	bdl	0.07	2.15	1.00	8.48	0.48	1.15	0.69	bdl	bdl	0.01	1.95	4.06	bdl
R.GO.3c	Yellowish naturally colored/Golden leaf	19.39	0.64	1.99	56.83	bdl	0.38	2.41	0.94	9.37	0.02	1.31	0.55	bdl	bdl	0.45	1.46	3.70	0.55
R.GO.4s	Greenish naturally colored/Golden leaf	18.88	1.03	1.67	58.22	0.03	0.18	2.31	1.08	9.29	0.41	1.53	0.97	0.01	bdl	0.09	1.54	2.76	bdl
R.GO.4c	Yellowish naturally colored/Golden leaf	18.02	0.68	2.37	60.65	0.17	0.65	3.19	0.59	9.65	0.05	0.93	0.42	bdl	0.12	bdl	0.17	1.79	0.55
R.S.1s	Greenish naturally colored/Silver leaf	16.65	0.72	2.16	60.86	bdl	0.45	2.10	1.05	9.54	0.43	2.23	1.08	bdl	0.25	bdl	0.74	1.73	bdl
R.S.1c	Yellowish naturally colored/Silver leaf	11.53	1.06	2.05	65.67	bdl	0.66	2.72	1.70	10.49	0.56	1.96	bdl	bdl	bdl	bdl	0.70	bdl	0.91
R.S.2s	Yellowish naturally colored/Silver leaf	14.96	0.49	1.97	61.08	0.34	0.75	2.40	1.20	10.94	bdl	1.95	1.15	bdl	0.49	0.39	bdl	0.67	1.24
R.S.2c	Yellowish naturally colored/Silver leaf	15.11	1.06	1.68	62.40	bdl	0.57	2.28	1.24	11.40	0.23	1.67	0.80	bdl	bdl	0.09	0.32	1.17	bdl
R.S.3s	Yellowish naturally colored/Silver leaf	13.85	0.67	1.73	62.43	0.08	0.79	2.53	0.71	12.97	0.07	2.51	0.06	bdl	bdl	0.49	bdl	0.78	0.36
R.S.3c	Yellowish naturally colored/Silver leaf	14.61	0.36	1.34	60.57	0.12	0.74	3.13	0.94	9.61	0.26	2.07	2.05	bdl	bdl	0.30	0.44	2.00	1.46

* Sample excluded from average values of Table 4.

Table 4. Average and min–max values in weight per cent oxides (wt%) of the Rotunda's colored and metal leaf tesserae (samples with sign * of Tables 2 and 3 were excluded). Outliers are excluded from average calculations.

		Na_2O	MgO	Al_2O_3	SiO_2	P_2O_5	SO_3	Cl	K_2O	CaO	TiO_2	MnO	Fe_2O_3	CoO	CuO	ZnO	SnO_2	Sb_2O_3	PbO
Colored	Average	15.25	0.75	2.11	54.08	0.29	0.31	2.49	1.51	10.41	0.15	0.33	1.20	0.11	1.06	0.16	1.93	1.38	6.48
	min	9.56	0.27	1.29	45.15	0.00	0.00	0.00	0.40	5.53	0.00	0.00	0.00	0.00	0.00	0.00	0.00	0.19	0.00
	max	24.35	1.94	2.89	62.94	0.96	1.11	4.64	2.82	17.92	0.38	1.35	3.97	1.01	2.64	1.25	5.93	4.40	16.47
Metal leaf	Average	17.11	0.73	1.89	60.07	0.13	0.47	2.52	1.05	9.55	0.28	1.64	0.75	0.01	0.07	0.23	0.93	2.11	0.44
	min	11.53	0.36	1.34	56.83	0.00	0.00	2.10	0.59	7.26	0.00	0.93	0.06	0.00	0.00	0.00	0.00	0.00	0.00
	max	20.56	1.06	2.37	65.67	0.36	0.79	3.19	1.70	12.97	0.67	2.51	2.05	0.03	0.49	0.49	1.81	4.06	1.46

The tesserae are characterized by various levels of potassium and magnesium (Tables 2 and 3). Potassium varies from 0.40% to 2.82% with an average of 1.35%. The potash concentrations in the R.B.L.3 and R.GO.2c samples (4.24% and 4.41%, respectively) are not representative, due to weathering phenomena affecting the glass, as mentioned above. For this reason, they were excluded from average values. However, in about half of the samples, the percentages of potassium are higher than expected in silicate glasses in which natron is used as a flux, the main flux used until the 8th-9th centuries, but still below the levels which characterize medieval potash-silica glass [25,33]. In the MgO vs. K_2O diagram (Figure 3) the majority of Rotunda's samples are included in the compositional space of natron glass, with the exception of the samples R.B.L.3, R.B.D.3, R.BR.1, R.BL.3 and R.GO.2c, from which samples R.B.L.3, R.B.D.3 and R.GO.2c have already been mentioned as outliers. The elevated K_2O concentrations (in connection with MgO) could be related to a secondary manufacturing process of the glass, during which the addition of colorants and opacifiers results in an introduction of plant ash to the batch [34–36]. This process could lead to potash enrichment of the glass as Paynter states [37]:

> *"The alkali-rich waste gases in wood-fired glass working furnaces can affect the composition of the glass when it is heated over prolonged periods. This results in increased concentrations of alkali, potash in particular".*

This technological feature is generally observed in the general group of red/orange/brown tesserae of many assemblages (see Section 4.7 of brown tesserae and references therein).

Concentrations of MgO higher than 1.5% are connected with the use of plant ash too [33]; however, in the Rotunda samples, MgO is generally below 1.0% (Figure 3) with the exception of samples R.BL.2, R.BL.3 and the outlier sample R.B.D.3.

Chlorine concentrations are higher than expected (average 2.47%) in comparison with the Cl values found in the typical groups of natron glass [38,39]. Phosphorus levels show a wide variation. In general, the higher values are noticed in samples with elevated potash concentrations, indicating the use of plant ash in the manufacturing process [38,40–44].

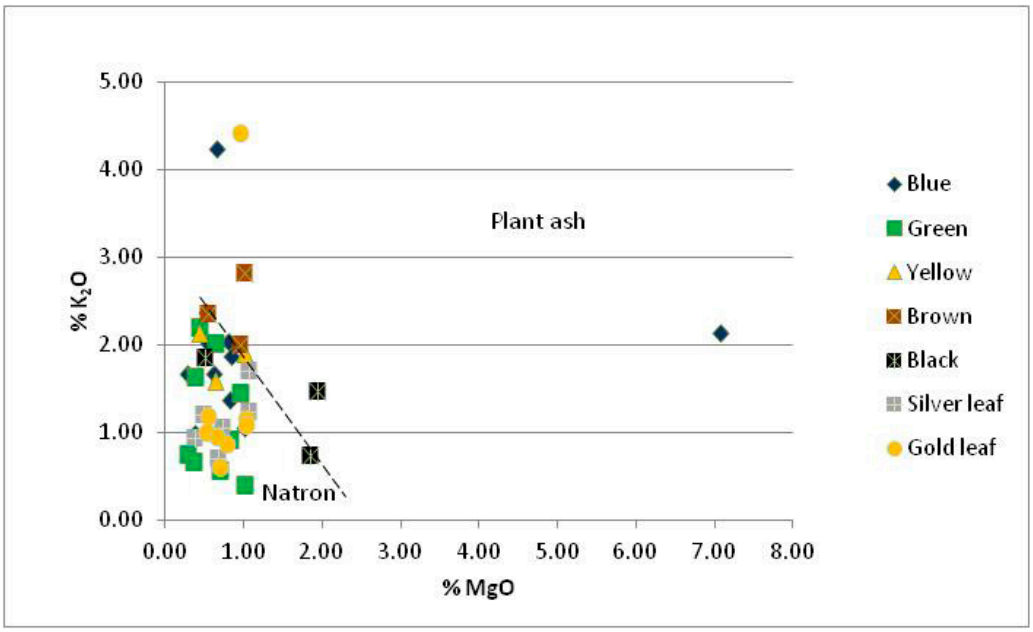
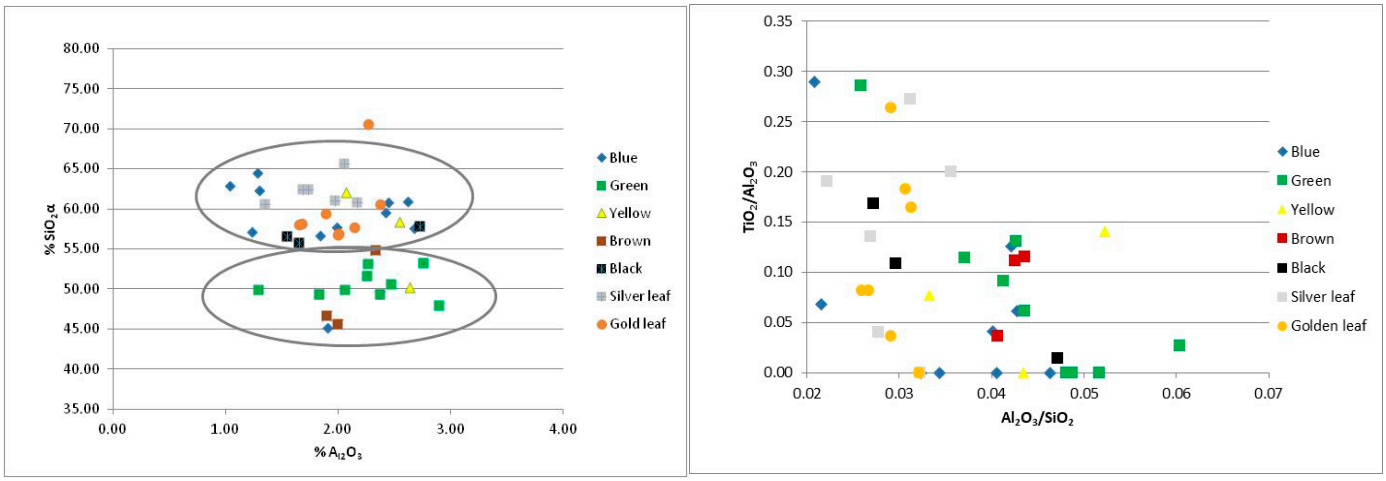


Figure 3. MgO vs. K_2O diagram of Rotunda samples. The dotted line separates the areas of natron and plant ash after [39].

In the Rotunda samples, silica levels vary between 45.15% and 65.67%, with an average of 56.75%. Two subgroups could be distinguished in the Al_2O_3 vs. SiO_2 diagram (Figure 4a).

In the first subgroup, with silica levels between 45 and 55%, belong the green, the brown, one yellow (R.Y.3) and one blue tessera (R.B.D.1). The second subgroup presents silica levels between 55% and 65% and includes the blue (except for R.B.D.1), the yellow (except for R.Y.3), the black, the gold leaf (except for R.GO.2c which is an outlier) and the silver leaf tesserae. The alumina concentrations in the samples for each color group vary between 1% and 3%. In addition to Al_2O_3 concentrations, Fe_2O_3, TiO_2 and CaO concentrations present variations which are indicative of different raw material sources, as they reflect the primary composition of the sand used and its impurities [39]. In the TiO_2/Al_2O_3 vs. Al_2O_3/SiO_2 diagram (Figure 4b), which is presented to discriminate between the main glass groups of the first Millennium in the Mediterranean area [39], no grouping is recognized for the Rotunda's glass tesserae. On the contrary, the samples are distributed among glass groups of different origins, without forming a compact group or subgroups, indicating compositional differences resulting from glass recycling.



(**a**) (**b**)

Figure 4. (**a**) SiO_2 vs. Al_2O_3 diagram and; (**b**) TiO_2/Al_2O_3 vs. Al_2O_3/SiO_2 diagram of the Rotunda samples.

Lime concentrations vary between 5.53% and 17.92% with an average of 10.03%. The slight elevation in the Ca values found in blue, brown and black samples, in conjunction with the others (Figure 4b), is connected with the presence of bone ash [45] and calcite, estimated using the SEM-EDS and XRD results (Table 5).

Table 5. Colorants, opacifiers, decolorizers and XRD crystalline phases identified in Rotunda's tesserae.

Sample Code	Color	Colorant/Opacifier/Decolorizer (SEM-EDS)	XRD Crystalline Phases
R.B.L.1	Light blue	Co, Cu, calcium phosphate, bubbles	Calcite
R.B.L.2	Light blue	Cu, calcium phosphate, bubbles	-
R.B.L.3	Light blue	Co, Cu, bubbles	Calcite, hillebrandite, combeite, quartz, galena, Sb_2SnZn
R.B.L.4	Light blue	Cu, calcium phosphate	Calcite, chabazite
R.B.L.5	Light blue	Co, Cu, bubbles	-
R.B.M.1	Blue	Co, Cu, calcium phosphate, bubbles	Calcite, chabazite
R.B.M.2	Blue	Cu, bubbles	Calcite
R.B.M.3	Blue	Co, Cu, bubbles	Calcite, Sb_2O_3, CuSn
R.B.D.1	Dark blue	Co, Cu, bubbles	Calcite, chabazite, CuSn
R.B.D.2	Dark blue	Co, Cu, bubbles	-

Table 5. *Cont.*

Sample Code	Color	Colorant/Opacifier/Decolorizer (SEM-EDS)	XRD Crystalline Phases
R.B.D.3	Dark blue	Cu, bubbles	Calcite
R.G.L.1	Light green	Cu, quartz, lead stannate, bubbles	Quartz, $CaPbO_3$, $PbSnO_3$
R.G.L.2	Light green	Quartz, lead stannate, bubbles	Quartz, $CaPbO_3$
R.G.L.3	Light green	Cu, quartz, lead stannate, bubbles	Quartz, $CaPbO_3$
R.G.M.1	Green	Cu, quartz, lead stannate, bubbles	Quartz, $CaPbO_3$
R.G.M.2	Green	Co, Cu, quartz, lead stanate, bubbles	Quartz, $CaPbO_3$
R.G.M.3	Green	Cu, quartz, lead stannate, bubbles	PbO_2, PbO, Pb_3O_4, chabazite
R.G.D.1	Dark green	Co, Cu, quartz, bubbles	Quartz, $CaPbO_3$, SnO_2
R.G.D.2	Dark green	Cu, quartz, lead stannate, bubbles	Quartz, calcite, $CaPbO_3$
R.G.D.3	Dark green	Cu, quartz, bubbles	Quartz, $CaPbO_3$
R.Y.1	Yellow	Co, Cu, cassiterite, lead stannate, bubbles	Quartz, $CaPbO_3$, PbO_2
R.Y.2	Yellow	Cassiterite, quartz, lead stannate, bubbles	Quartz, calcite, chabazite, PbO, PbO_2
R.Y.3	Yellow	Co, Cu, quartz, lead stannate, bubbles	Quartz, $CaPbO_3$
R.BR.1	Brown	Co, Cu, Fe, bubbles	Cu
R.BR.2	Brown	Co, Cu, Fe, bubbles	Cu, cassiterite, calcite, wollastonite, chabazite
R.BR.3	Brown	Co, Cu, Fe, cassiterite, bubbles	Cu, calcite, chabazite
R.BL.1	Black	Co, Cu, Fe, cassiterite, bubbles	
R.BL.2	Black	Cu, Fe, cassiterite, bubbles	Calcite, coesite
R.BL.3	Black	Cu, Fe, bubbles	
R.GO.1	Gold leaf	Sb/Mn	
R.GO.2	Gold leaf	Mn	
R.GO.3	Gold leaf	Sb/Mn	
R.GO.4	Gold leaf	Sb/Mn	
R.S.1	Silver leaf	Sb/Mn	
R.S.2	Silver leaf	Sb/Mn	
R.S.3	Silver leaf	Sb/Mn	

Concerning lead concentrations, the glass tesserae were classified according to the ratio between lead and the sum of silicon, sodium and calcium concentrations expressed as PbO, SiO_2, Na_2O and CaO [1,46,47]. Three categories are recognized:

1. Soda–lime, when the $PbO/(SiO_2+Na_2O+CaO)$ ratio is less than 0.01.
2. Soda–lime–lead, when the $PbO/(SiO_2+Na_2O+CaO)$ ratio is between 0.01 and 0.1.
3. Leaded, when the $PbO/(SiO_2+Na_2O+CaO)$ ratio is higher than 0.1.

The Rotunda samples are distributed across these three categories, with the most numerous being the soda–lime group (20/43 measurements) which includes the majority of the metal leaf tesserae, the majority of the blue tesserae and the black tesserae. Leaded glass tesserae are the second most numerous category (14/43 measurements) including all the green tesserae, the majority of the yellow and brown tesserae and one blue tessera. Lead in the leaded tesserae plays a significant role in color which is attributed to the presence of yellow lead stannate. The soda-lime-lead category counts nine (9) samples sporadically distributed into the different color groups.

4.2. Coloring, Opacifying and Decolorizing Elements

The transparent glass of the gold and silver leaf tesserae is unintentionally green and yellow colored, due to iron impurities included in the raw materials. On the contrary, all the other tesserae are intentionally colored using metal elements in different amounts and oxidation states (Table 5). Copper, iron, cobalt, and manganese, along with colored compounds of lead, tin and calcium, are responsible for the variety of the glass tesserae's hues. Tin compounds have been detected in many samples and are responsible for both

the coloration and opacification of the glass. In the colored samples, bubbles, bone ash inclusions and quartz relics contribute to their opacification. Although antimony-rich inclusions have not been detected, except for Sb_2O_3 in the XRD pattern of R.B.M.3, antimony concentrations in many of the samples are very high and, in many cases, exceed manganese concentrations. Manganese is absent or is detected in low concentrations in most colored samples, in contrast to the gold and silver leaf tesserae, in which manganese concentrations are higher and similar to antimony ones. According to concentration thresholds for characterizing colorless glass as Sb, Mn or Sb/Mn decolorized, the glass used in most of the Rotunda's tesserae belongs to the Sb/Mn-decolorized group. Sb/Mn-decolorized glass is the result of the two other groups' mixing in a recycling process, according to the literature [39,48]. In this recycled Sb/Mn-decolorized glass, a new technological trend in the period, tin-rich compounds, were added to opacify or color the glass [49].

Coloring elements, opacifiers and decolorizers are discussed analytically per color group in the following sections.

4.3. Blue Tesserae

All blue samples contain variable amounts of copper, in addition to cobalt. Cobalt is generally considered as the primary chromophore for blue coloration, while Cu does not show a strict correlation with the hue, because of the lack of consistency between Cu content and blue color intensity. Cobalt exists in all the samples apart from R.B.L.2, R.B.L.4, R.B.M.2 and R.B.D.3. Sample R.B.L.3 exhibits a questionably high Co concentration (2.42%), taking into account the strong coloration effect of the element and the pale color of the sample [50]. In the blue tesserae color group, lead exists in negligible amounts except for in two samples of darker hue (R.B.D.1, R.B.D.2).

In four blue samples (R.B.L.1, R.B.L.2, R.B.L.4, R.B.M.1), the three being of lighter hue, BSE images revealed the presence of inclusions rich in Ca-P (Figure 5), indicating the use of calcium phosphate (bone ash) as an opacifier and a color affecting agent, a feature connected mainly with glass production of the Levantine area [51]. Bone ash, cheap and easily available, has been used as an occasional glass opacifier from the fifth century onwards, substituting the more expensive Ca-antimonates and Ca-stannates [52], although its use is testified from the 2nd century [53]. Opacifier grains, micro-textural features and the stages of the process have been described in detail by Silvestri et al. [54] and Maltoni and Silvestri [52]. Their main structure includes calcium phosphate (mineral hydroxyapatite-$Ca_5(PO_4)_3(OH)$) in lighter areas surrounded by a rim of darker hue, where the sodium in the glass matrix replaces the calcium from the opacifier. In sample R.B.L.4, a similar inclusion presents lighter and darker areas without clear concentration correlations, although in the darker areas the sodium concentration is higher (Figure 5a). No newly formed crystallites have been detected by BSE imaging of the Ca-P grains. However, wollastonite, a mineral connected to cation replacement in Ca-P grains [54], has been detected in the XRD pattern of sample R.B.L.5. Grains of smaller size have a more uniform structure (Figure 5b). Bubbles are closely connected to the opacifier grains and their presence is attributed to the opacifier's decomposition [51,52]. The exclusive use of this opacifier in blue tesserae is also mentioned in other assemblages [1,40,55].

According to the collected XRD patterns—as the identified phases are presented in Table 5—and apart from the pronounced amorphous matrix, calcite can been identified in eight (8) samples and is attributed to traces of the mosaic mortar substrate. In sample R.B.M.3, the identified copper–tin phase is connected to the mineral source of copper, while the presence of antimony oxide could not be directly connected to its use as an opacifier. Finally, silicate minerals (chabazite, quartz, combeite, and hillebrandite)—sporadically identified—(Figure 6 as representative) are either relics of the raw materials,

intentional additions which contribute to opacification (e.g., quartz [56]) or devitrification products [57].

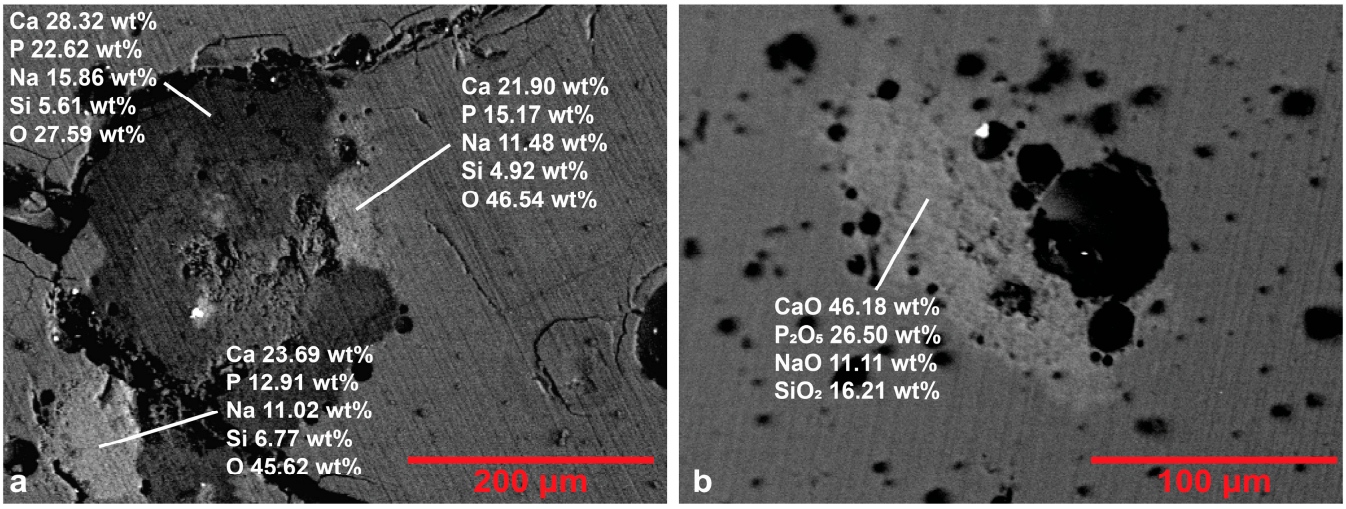


Figure 5. Representative BSE images of blue samples from areas presenting inclusions: (**a**) R.B.L.4, and (**b**) R.B.M.1.

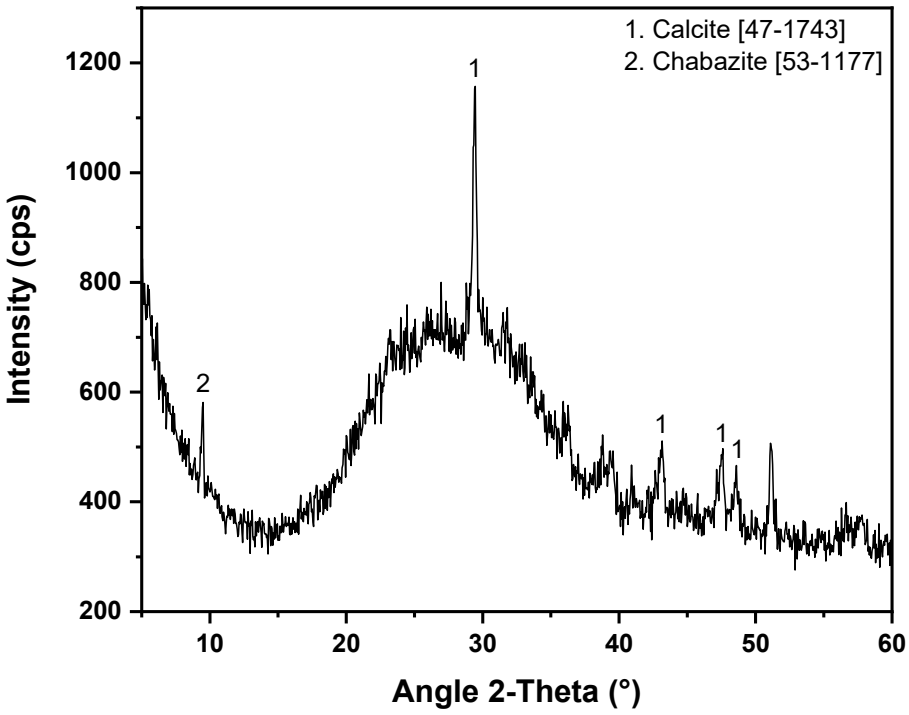


Figure 6. XRD pattern of the light blue tessera R.B.L.4. The JCPDS-ICDD reference cards used for phase identification are indicated.

4.4. Green Tesserae

Figure 7 shows BSE images and an XRD pattern of representative green tesserae under study. All green tesserae are made of leaded glass. They include, except for R.G.L.2, various amounts of copper, which contributes to the color shade. In a BSE image of the sample R.G.D.1, copper was detected in the form of a carbonate mineral, probably malachite (Figure 7b). In only two samples (R.G.M.2, R.G.D.1) of darker hue were traces of cobalt detected. In every case, the higher the concentration of cobalt, the darker the hue of the sample. In all green samples, high amounts of lead have been

detected, varying between 12.00% and 18.59%. Lead in conjunction with tin—as the Pb-Sn-rich inclusions found in BSE images (Figure 7a,c as representative) in eight tesserae indicate—forms yellow lead stannate which, together with the blue cupric and cobalt ions, contributes to the green color and the glass opacity. In BSE images, sample R.G.M.3 exhibits stripes of darker and lighter hue with no detectable chemical distinction between the different glass matrices. The abundance of lead stannate particles, unevenly distributed among the stripes (Figure 7c), confirm their introduction after the mixing of the different glass matrices [44]. In almost all green samples, crystalline phases of calcium lead oxide ($CaPbO_3$) and quartz have been detected via XRD analysis (Figure 7d as representative, and Table 5). Particularly in the XRD pattern of R.G.L.1, as presented in Figure 7d, besides the pronounced amorphous matrix and the participation of $CaPbO_3$, the presence of $PbSnO_3$ is indicated from the observed broadening and the appearance of secondary peaks and shoulders, due to partial overlap or reflections occurring at nearby diffraction angles. BSE images confirmed the presence of quartz relics in the majority of the samples. Lead stannate, quartz and the abundance of bubbles found in all green samples are responsible for the glass' opacity [21]. Quartz relics and bubbles are considered as an alternative opacifier when other opacifiers are absent [50]. In the case of the Rotunda, they contribute to the opacity together with a tin-based opacifier. Calcium lead oxide is rather a byproduct of the glass manufacture process [58].

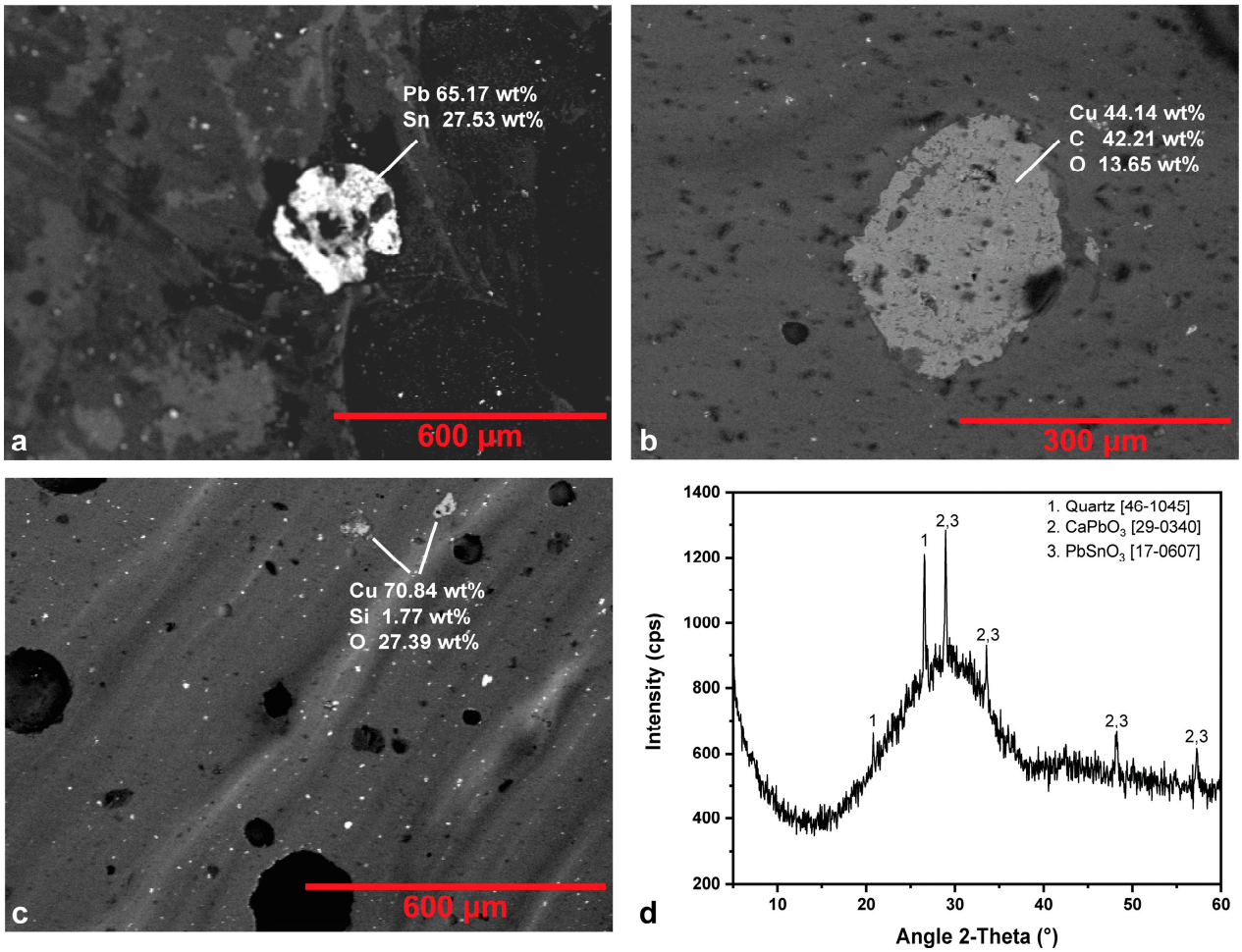


Figure 7. Representative BSE images of green tesserae from areas presenting inclusions: (**a**) R.G.L.1, inclusion of lead stannate, (**b**) R.G.D.1, Cu-rich inclusion, (**c**) R.G.M.3, lead stannate dispersed inclusions (white hue) and two Cu-rich inclusions; (**d**) XRD pattern of R.G.L.1. The JCPDS-ICDD reference cards used for phase identification are indicated.

4.5. Yellow Tesserae

All yellow tesserae have a greenish tint and similar morphological characteristics to the green samples. Small amounts of copper and cobalt have been detected in samples R.Y.1 and R.Y.3 by EDS analysis, contributing to the greenish tint they present, while in sample R.Y.2 neither of these two elements was detected. SEM-EDS results indicate the presence of lead stannate agglomerates in the three yellow samples, together with quartz relics (Figure 8a). Yellow lead stannates are considered as a typical Byzantine trend in glass opacification [1], however they are occasionally found in Roman glass of Eastern Mediterranean [51,59]. A fine powder of lead-tin calx, which contained also PbO, SnO_2, SnO, Pb and Sn except for Pb_2SnO_4, was mixed with silica, silica and alkalis, or a prepared glass frit, to produce a yellow-colored glass. The stages of the process and the parameters that influence the chemical composition and the color of the final product are described by Tite et al. [60] and Matin [59]. XRD results confirmed the presence of quartz, calcium lead oxide and lead oxide (Figure 8b, Table 5).

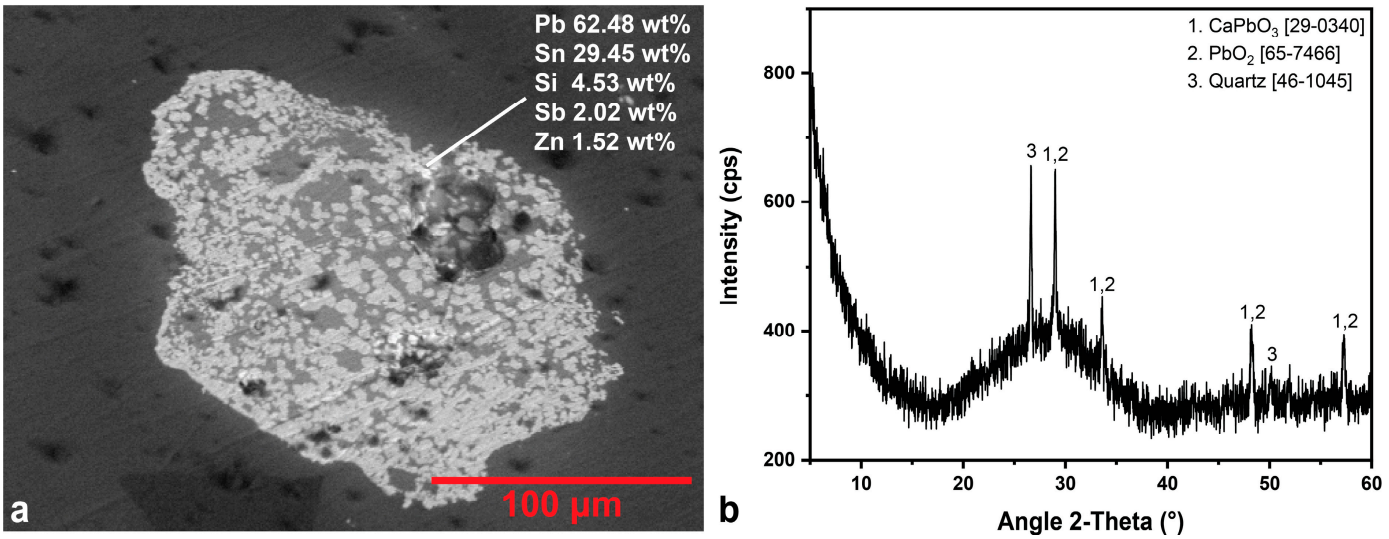


Figure 8. (**a**) BSE image of an inclusion detected in yellow sample R.Y.3. Its elemental analysis indicates the agglomeration of lead stannate particles. (**b**) XRD pattern of R.Y.1. The JCPDS-ICDD reference cards used for phase identification are indicated.

4.6. Black Tesserae

Black tesserae exhibit elevated sodium concentrations in two of the three samples and negligible amounts of lead. The samples are characterized by heterogeneity in color, with greenish areas distributed in dark glass matrix (Figure 9a as representative), as it has been observed in other black glass tesserae [40,61]. According to L*a*b* color diagram (Figure 2), they are distributed among dark blue and dark green samples despite their black, perceived to the naked eye, color. In sample R.BL.2, an iron-rich inclusion has been detected by SEM-EDS analysis (Figure 9b). This sample exhibits the highest content of iron which contributes to its color, as the combination of blue Fe^{+2} and yellow Fe^{+3} ions in the glass matrix result to the green shade, observed in many areas of the sample [62].

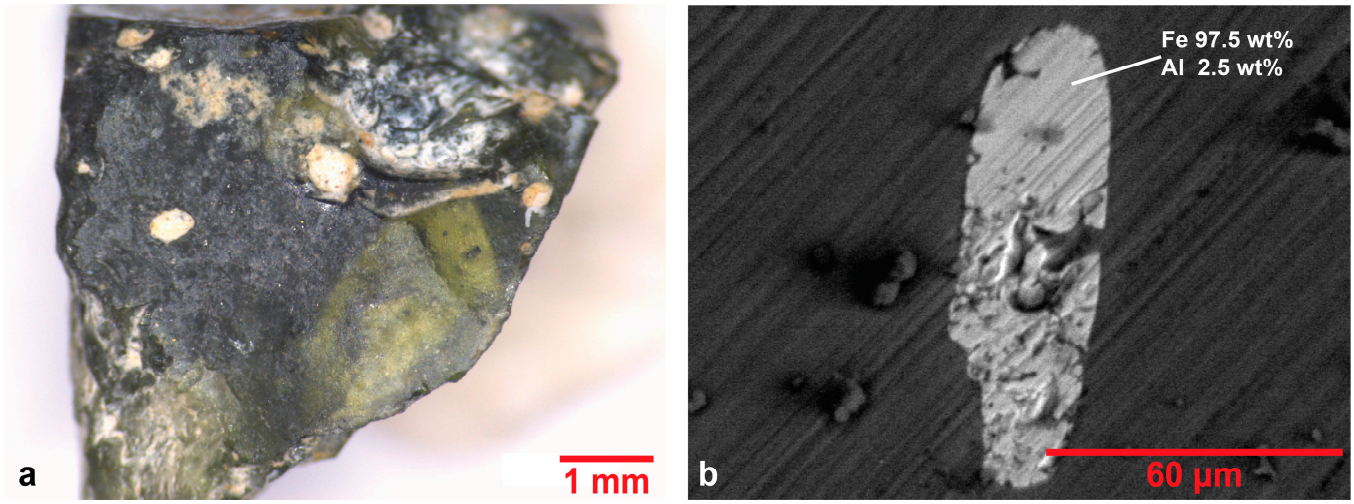


Figure 9. (**a**) Optical image of black sample R.BL.2. The presence of greenish areas among dark glass matrix is noted. (**b**) Representative BSE image of an inclusion rich in iron detected in black sample R.BL.2.

4.7. Brown Tesserae

Two of the three brown samples (R.BR.2, R.BR.3) are banded with areas of brighter and darker colors (Figure 10a as representative). Although the stripes are observed macroscopically, in the BSE images only in R.BR.2 is a slight shade differentiation observed, with no compositional or textural heterogeneity, suggesting a homogeneous chemical composition of the glass, unlike in other assemblages [49,51,63–66]. This feature was observed in brown tesserae from two other monuments in Thessaloniki [67].

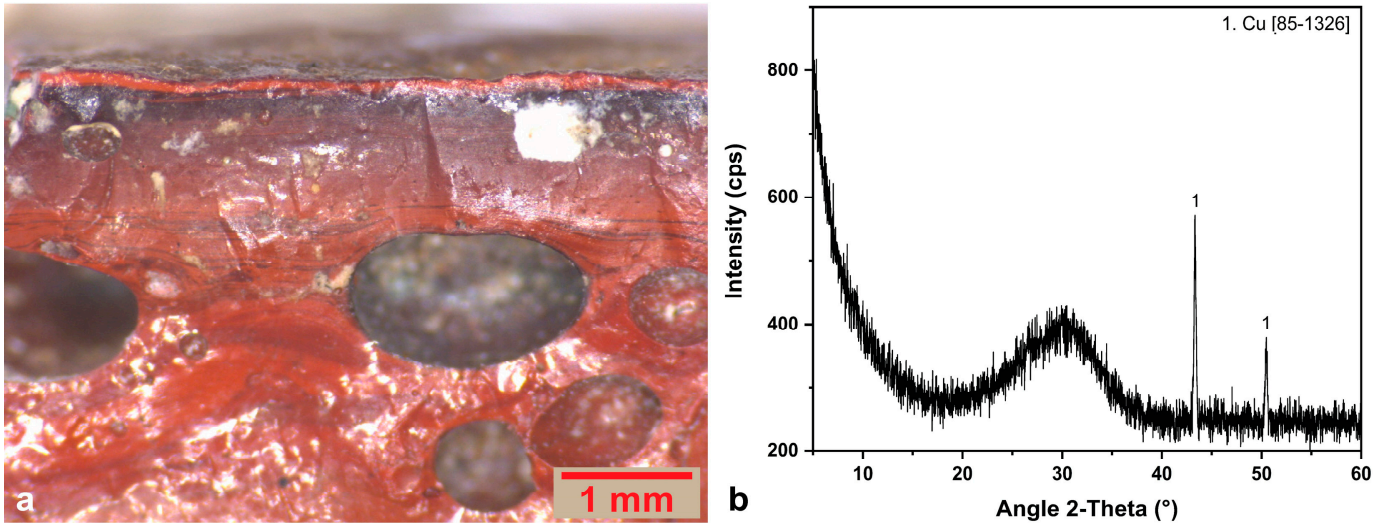


Figure 10. (**a**) Optical image of brown sample R.BR.3, as received. (**b**) XRD pattern of the brown tessera R.BR.1. The JCPDS-ICDD reference card used for phase identification are indicated.

In all brown samples, different amounts of copper were detected by EDS. Furthermore, metallic copper has been detected in all brown samples via XRD analysis (Figure 10b as representative). Metallic copper or cuprite are responsible for red/orange/brown color in glass [68,69]. As regards brown glass, metallic copper is responsible for the hues when the concentrations of copper and lead are relatively low [64,70]. In the case of Rotunda's brown tesserae, copper levels are rather low, and the lead contents are elevated in two of the three samples, but not enough to favor the formation of cuprite dendritic structures that are responsible for an orange/red hue [40,69]. SEM-EDS analysis of the inclusions detected

in both samples R.BR.1 and R.BR.3, indicates that copper coexists with high amounts of sulfur (Figure 11a,b), referring to the mineral source relics of copper as it has been stated for other assemblages [36,63,71]. According to our bibliography, lead improves the nucleation and growth of metallic copper crystallites, while no specific lead amounts are needed for stimulating the precipitation of metallic copper [69,72]. The elevated concentrations of iron (2.69–3.97%), tin (1.77–5.57%) and antimony (0.35–1.93%) in brown tesserae suggest their intentional use as reducing agents for copper [34,50,63,66,68–70].

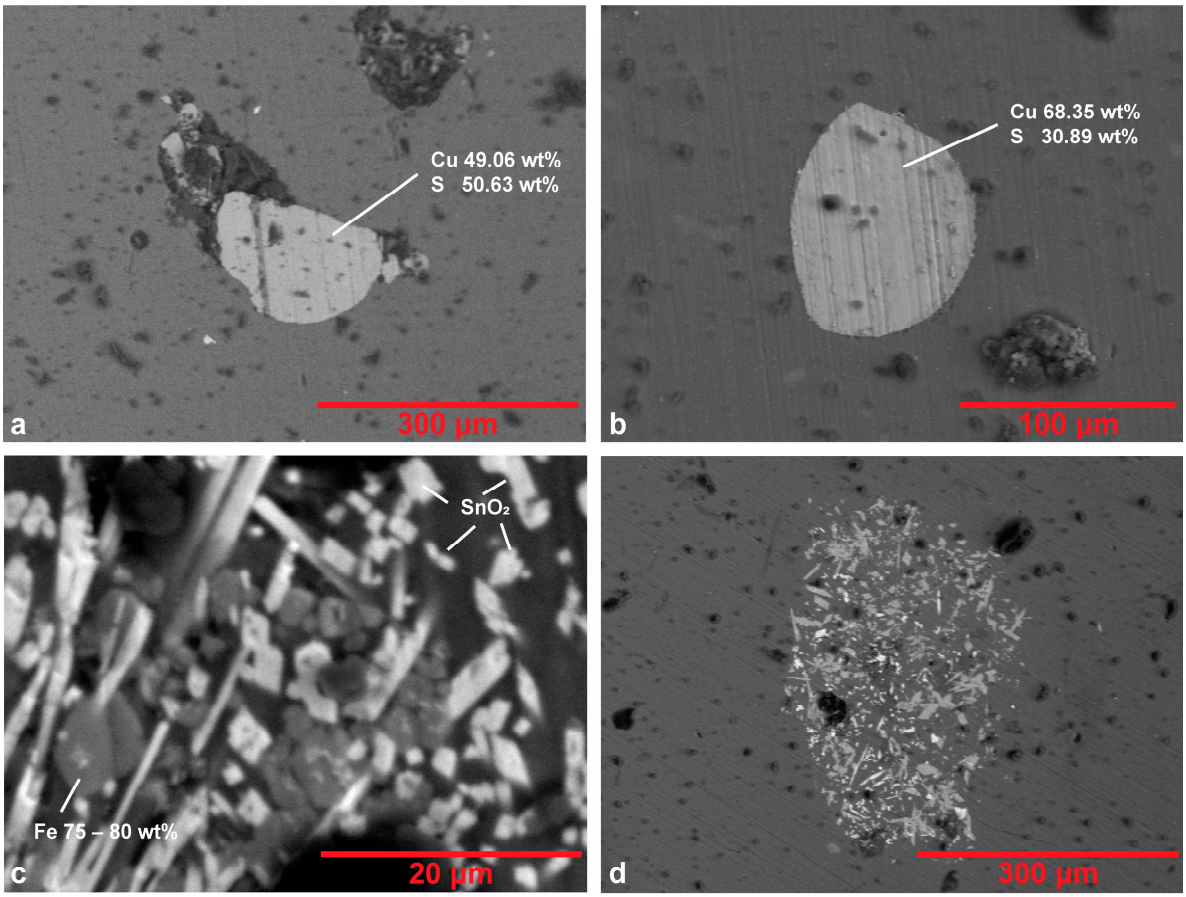


Figure 11. Representative BSE images of brown tesserae from areas presenting inclusions: (**a**) Cu-S-rich inclusion in sample R.BR.3. (**b**) Cu-S-rich inclusion in sample R.BR.1. (**c**) Clusters of well-defined, angular SnO_2 crystallites and rounded Fe structures in sample R.BR.1. (**d**) Clusters of well-defined, angular SnO_2 (white) and $Ca_3SnSi_2O_9$ (gray) crystallites in sample R.BR.2.

The Rotunda' s brown samples have high potassium concentrations (2.01–2.82%), which can be attributed to the use of plant ash in the manufacturing process. For the brown tesserae in this category, plant ash is often used as a source of alkali as stated in other cases [35,40,73,74], or as additional fuel ash in a natron based glass -adding extra carbon- to obtain the wanted reducing conditions for coloring [2,40,44,50,70,72,75,76].

Euthedral cassiterite crystallites were observed in abundance in BSE images of samples R.BR.1 and R.BR.2. In addition, the XRD analysis of the sample R.BR.2 confirmed the presence of cassiterite (Table 5) [67]. In these samples, cassiterite coexists with darker Fe- or Ca-Sn-Si-rich crystallites (Figure 11c,d), the latter contribute intentionally to the glass opacification or are a devitrification product [53,68]. Cassiterite has generally been used as an opacifier from the fourth century onwards and it is recognized as a special production marker [56,77,78]. It was used in glasses colored with other colorants such as metallic copper [59].

4.8. Gold Leaf Tesserae

Figure 12 shows representative images of gold leaf tesserae, collected by means of optical and electron microscopy. All the gold leaf samples except for R.GO.2 show in cross sections the sandwich arrangement (supporting glass–gold leaf–*cartellina*), characteristic of metal leaf tesserae [21,79]. On the back side they preserve a rough surface made from the refractory powder used to prevent glass from sticking to the manufacturing sub board when pressed on it during manufacturing [80]. In particular, sample R.GO.3 shows traces of a red pigment, probably belonging to the initial sketch of the mosaic composition (Figure 12a).

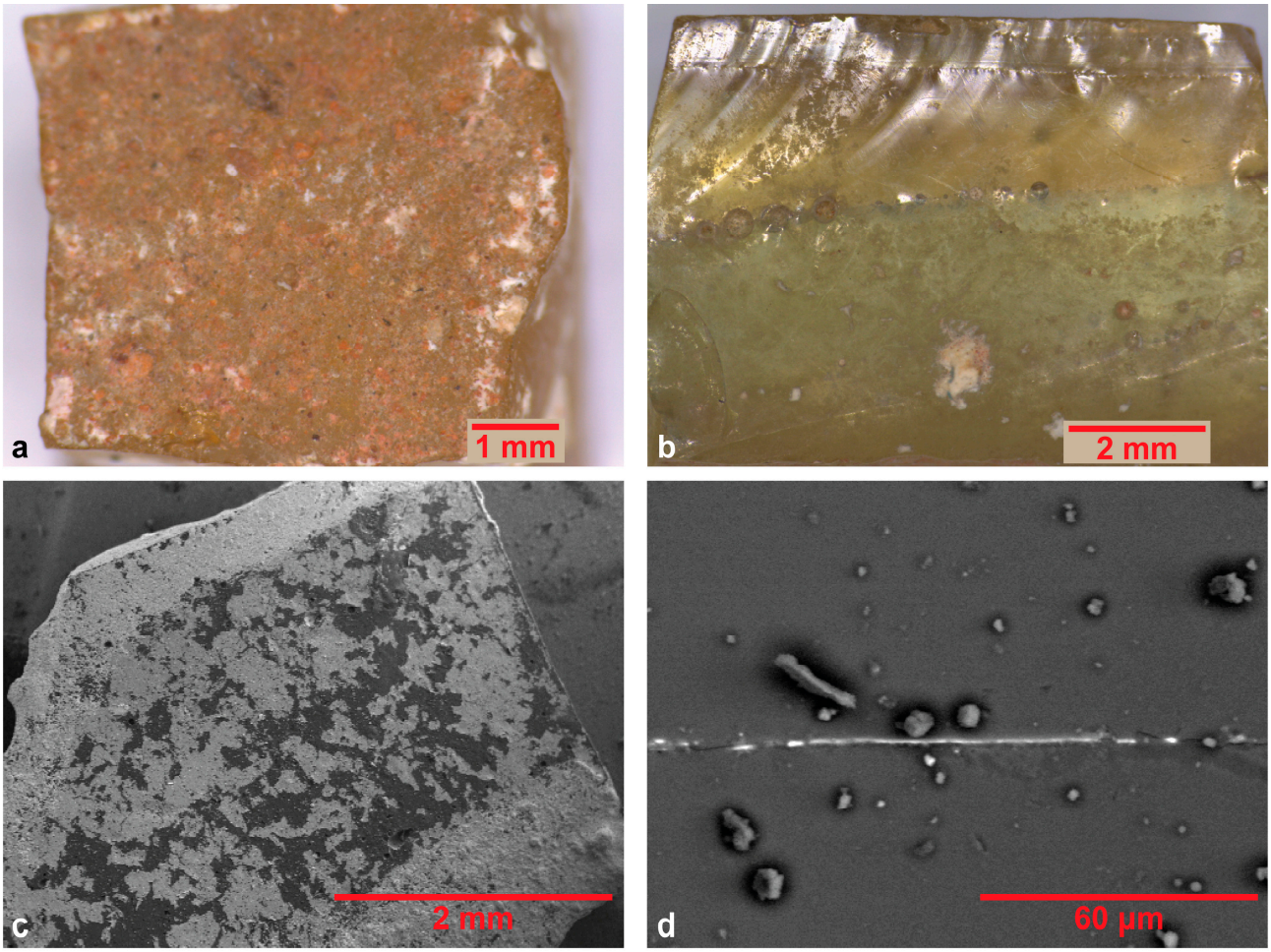


Figure 12. Optical microscopy images of (**a**) red pigment detected on the back side of the sample R.GO.3, and (**b**) the cross section of the sample R.GO.1, which demonstrates the mixing of two different glass matrixes in the support, one with a yellowish tint and one with a greenish tint. Representative BSE images of (**c**) sample R.GO.2, and (**d**) the gold leaf in the cross section of sample R.GO.1.

The transparent glass used for the manufacture of the gold leaf tesserae presents a soda content which varies between 18.02 and 20.56%, while the potash content varies between 0.59% and 1.18% (Tables 3 and 4). Considering the concentrations of manganese and antimony [81], all gold samples are characterized as Mn/Sb decolorized, except for sample R.GO.2c, in which Sb is absent. In all the other samples, Mn exists in lower concentrations than Sb. A natural yellowish or greenish tint is observed due to iron in the divalent or trivalent oxidation states, introduced to the batch unintentionally as impurities from the raw materials [79]. The hue of the glass matrix, indicative of the glass type used, is a random rather than a deliberate choice, as the three gold leaf tesserae (excluding R.GO.2c) represent three different situations:

- R.GO.3: Both *cartellina* and support glass have a yellowish tint.
- R.GO.4: *Cartellina* has a yellowish tint while the support glass is greenish.
- R.GO.1: *Cartellina* is yellowish, while both hues coexist in support glass.

In this case, two different glasses have been melted and mixed together, with air bubbles trapped in a linear arrangement between them (Figure 12b). Inevitably, the hue of the *cartellina* and the support glass influences the optical effect of the tesserae [20]; however, a mixture of gold and silver leaf tesserae, with different hues in the added glass, increases the visual interest of a monochrome part of a composition as the background. For this reason, a random choice of naturally colored glass for the manufacture of metal leaf tesserae does not really matter. On the contrary, it gives an optical advantage to the mosaic' composition.

The two glasses used in the support glass of R.GO.1 are Sb- and Mn-decolorized, and present a different chemical composition, as is confirmed mainly from their Si, Ca and Mg contents. The bubbles trapped between the two glasses are indicative of using cast rather than blown glass for the manufacture of the support, although the support glass in Rotunda samples generally presents homogeneity and a lack of bubbles in contrast with other cases [49,79,82]. *Cartellina*'s thickness is about 1 mm in all cases, while the thickness of the support glasses ranges from 5 to 5.9 mm. The three layers present a strong adherence to each other, especially where there is a lack of gold leaf, the thickness of which varies between 0.50 and 1 μm (Figure 12d). The gold leaf does not actually consist of pure gold, but it is, in all cases, an alloy with silver and copper, with a not negligible amount of sulfur. The latter is probably connected with the corrosion of silver or copper (Table 6). The concentration of gold (85.50–95.10%) in the golden leaves does not refer to a direct connection with golden coins as a source of the alloy [82], but it resembles jewelry alloys [83].

Table 6. Gold and silver leaf composition (wt%) of the gold and silver samples.

Sample	S	Cu	Ag	Au	Sn	Zn	Fe	Pb
R.GO.1	3.26	0.26	2.33	94.15	-	-	-	-
R.GO.2	0.84	0.21	3.85	95.10	-	-	-	-
R.GO.3	1.17	0.11	4.17	94.55	-	-	-	-
R.GO.4	2.87	4.55	7.07	85.50	-	-	-	-
R.S.1	0.79	-	95.82	-	1.44	-	-	1.96
R.S.2	-	0.79	89.25	0.38	8.45	-	1.13	-
R.S.3	0.37	0.03	86.43	-	12.92	0.25	-	-

4.9. Silver Leaf Tesserae

The silver leaf tesserae of Rotunda have the same cross section arrangement as the one described for the gold leaf ones. On the back side they also preserve the rough surface made from the refractory powder used to prevent glass from sticking to the manufacturing sub board (Figure 13a). The soda contents vary between 11.53% and 16.65% (Tables 3 and 4). According to the potassium and magnesium contents of the category, the glass used for their manufacture belongs to the glass type that uses natron as a fluxing agent (Figure 3). In R.S.2 and R.S.3 samples, a naturally colored, yellowish, transparent glass has been used both for *cartellina* and support, while, in R.S.1, a transparent glass with yellowish tint has been used for *cartellina*, and a transparent glass with greenish tint has been used for the support. The glass with the greenish tint does not exhibit an obvious differentiation in composition in comparison to the others with the yellowish tint. Silver leaf tesserae are made of recycled Sb- and Mn-decolorized glasses, except for R.S.1c, which is Mn-decolorized. Significant differences in oxide concentrations (of Na, Mg, Fe, Sb, Ca) between support glass and

cartellina in the three samples indicate the use of different raw glasses within the same tessera. *Cartellina*'s thickness ranges from ~0.5 to 1 mm, while the support's glass thickness ranges from ~4 to ~5.5 mm. The silver leaf is about 0.50–1 μm thick and consists of an alloy with silver content ranging from 86.43% to 95.82%. Other elements detected in small amounts in the metallic leaves are S, Sn, Cu, Zn, Au, Pb and Fe (Table 6).

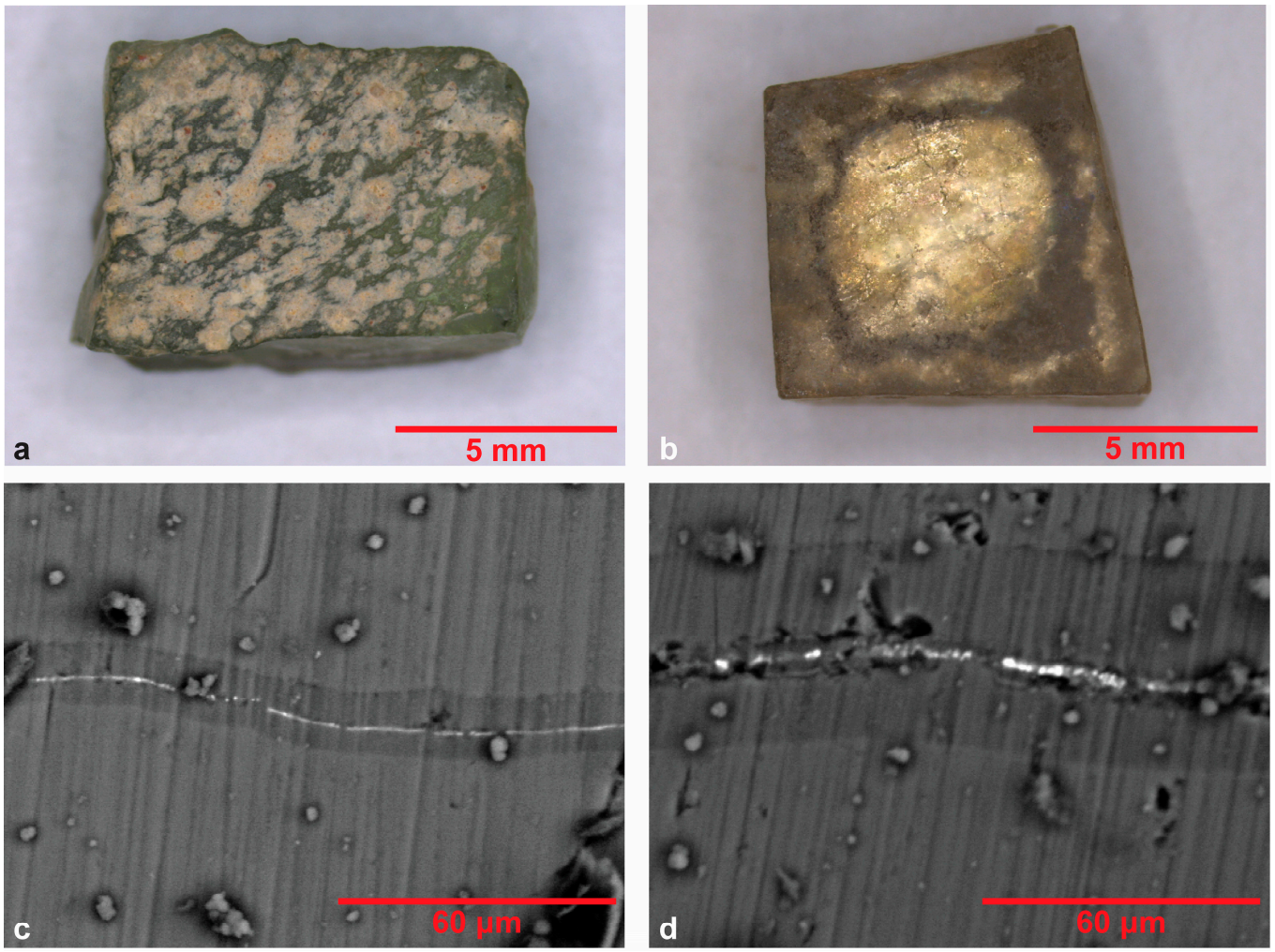


Figure 13. Optical microscopy images of (**a**) back side of R.S.1, (**b**) the front side of the silver tessera R.S.3, where a dark "crown" on the periphery of the silver leaf is observed. BSE images of cross-sections of (**c**) R.S.2 and (**d**) R.S.3, where a zone of darker hue is observed on either side of the silver leaf.

In two of the silver leaf samples (R.S.2, R.S.3), a zone of darker hue is observed in BSE images on either side of the silver leaf (Figure 13 c,d). A dramatic decline in Na concentration and an increase in Si and K concentrations are noticed in the chemical composition of this zone, compared to the rest of the studied glass cross-sections. In R.S.2 an additional increase in Mn and S content is observed. This chemical differentiation is attributed to the glass deterioration in conjunction with the corrosion of the silver alloy and in contact with environmental deterioration parameters. A black "crown" observed macroscopically around the periphery of the R.S.3 tessera is probably connected to the darker zones of the SEM images (Figure 13b). Loukopoulou describes similar chemical alterations of the glass called "manganese staining" in the interface with the metallic leaf [29].

5. Conclusions

According to the obtained data, the Rotunda's tesserae are composed of soda-lime-silica glass, in which a mineral source of alkali was used. In most samples, the primary glass belongs to the Sb- and Mn-decolorizing category, suggesting that it results as a product from the recycling of Sb-decolorized and Mn-decolorized glass. Glass recycling was a common practice from Late Antiquity onwards [41], and in this assemblage, it is evidenced by the simultaneous presence of the two decolorizers. The use of two different glass types in the support glass of the gold leaf tessera R.GO.1. further supports this interpretation. Out of the 36 tesserae analyzed, only 8 are solely Sb-decolorized, and one is Mn-decolorized.

In the primary glass, which was decolorized using antimony or manganese, colorants and opacifiers were added during a secondary manufacturing stage, to achieve the desired hues. During this stage, the introduction of plant ash led to an enrichment in potash content, which is observed in approximately half of the tesserae studied. Cobalt, copper, iron and manganese, together with lead and tin compounds, contribute to blue, green, yellow, brown, and black colors, respectively. In the fourth century, tin based opacifiers (such as cassiterite, calcium and lead stannate) gradually replaced antimony-based opacifiers, which were commonly associated with Roman glass production [33,34,40,50,51,66]. However, there is evidence that both types of opacifiers coexisted in glass manufacturing in earlier periods [35,60,72,76,84–89], enabling the production of a broader range of colors [90]. In the Rotunda samples, only tin-based compounds were identified via SEM-EDS and XRD analyses, in agreement with findings from other assemblages of the same period in Syria [40], Italy [49,50,76], Cyprus [1] and Albania [91]. Tin-based opacifiers, calcium phosphate, quartz relics, and bubbles cause light refraction and diffusion, which are responsible for the opacity of the colored tesserae. From the fifth century onward, the use of calcium phosphate as an opacifier became widespread in the eastern Mediterranean [1,21,51,76] and its presence in the Rotunda's tesserae indicates its earlier introduction to glass manufacturing.

The predominant theory about glass production and trade during the Roman and early Byzantine periods suggests the existence of a limited number of primary production centers in Egypt and Levantine coast. From these centers, glass was distributed to secondary glass workshops, to be colored and/or opacified, and, finally, be shaped into artifacts [39,92]. According to this theory, glass tesserae -being the final products- are expected to reflect the composition of the primary glass, enriched with colorants and opacifiers during secondary processing. The use of different recipes and opacifiers in the Rotunda's assemblage suggests the use of multiple primary glass sources and reflects the transition from the Roman glass tradition to the Byzantine glass production practices in the eastern Mediterranean during the fourth and the fifth centuries.

The analytical investigation of the Rotunda's glass mosaic tesserae provided significant insights into Byzantine mosaic production in Thessaloniki. Despite the variations in composition throughout the tesserae under study, mainly attributed to the use of recycled glass, many of their features are consistent with those observed in other Byzantine assemblages, establishing a broader chronological framework for the mosaic's composition.

Author Contributions: Conceptualization, M.K.; methodology, M.K., L.M., G.V., E.P. and K.C.; software, G.V. and E.P.; validation, M.K., L.M., G.V., E.P. and K.C.; formal analysis, M.K. and L.M.; investigation, M.K. and L.M.; resources, G.V., E.P. and K.C.; data curation, M.K.; writing—original draft preparation, M.K.; writing—review and editing, M.K., L.M., G.V., E.P. and K.C.; visualization, M.K. and L.M.; supervision, K.C. All authors have read and agreed to the published version of the manuscript.

Funding: This research received no external funding.

Data Availability Statement: The original data used for this study are included in the article. Further inquiries can be directed to the corresponding authors.

Acknowledgments: The authors are grateful to the Ephorate of Antiquities of Thessaloniki City for providing the archeological material and archive figures. The authors have reviewed and edited the output and take full responsibility for the content of this publication.

Conflicts of Interest: The authors declare no conflicts of interest.

Abbreviations

The following abbreviations are used in this manuscript:

Bdl	Below detection limit
BSE	Backscattered electron
CIE	Commission Internationale de l'Eclairage
ICDD	International Centre for Diffraction Data
JCPDS	Joint Committee on Powder Diffraction Standards
OM	Optical microscopy
PDF	Powder Diffraction Files
SEM-EDS	Scanning electron microscopy with energy dispersive spectroscopy
Std Dev	Standard deviation
XRD	X-ray diffraction
XRF	X-ray fluorescence

References

1. Bonnerot, O.; Ceglia, A.; Michaelides, D. Technology and materials of Early Christian Cypriot wall mosaics. *J. Archaeol. Sci.* **2016**, *7*, 649–661. [CrossRef]
2. Schibille, N.; Neri, E.; Ebanista, C.; Ramzi Ammar, M.; Bisconti, F. Something old, something new: The late antique mosaics from the catacomb of San Gennaro (Naples). *J. Archaeol. Sci. Rep.* **2018**, *20*, 411–422. [CrossRef]
3. Mastora, P.; Kyranoudi, M.; Zacharopoulou, G. Wall mosaics of Thessaloniki: Recording the art and technology of the archaeological findings. In Proceedings of the 14th Conference of the Association Internationale pour l'Étude de la Mosaïque Antique (AIEMA), Nicosia, Cyprus, 15–19 October 2018.
4. Velenis, G. Some observations on the original form of the Rotunda in Thessaloniki. *Balkan Stud.* **1974**, *15*, 298–307.
5. Mentzos, A. Reflections of the interpretation and dating of the Rotunda of Thessaloniki. *Egnatia* **2000**, *5*, 57–80.
6. Nasrallah, L.S. Empire and apocalypse in Thessaloniki: Interpreting the early Christian Rotunda. *J. Early Christ. Stud.* **2005**, *13*, 465–508. [CrossRef]
7. Torp, H. An interpretation of the early Byzantine martyr inscriptions in the mosaics of the Rotunda at Thessaloniki. *Acta Archaeol. Artium Hist. Pertin.* **2011**, *24*, 11–43. [CrossRef]
8. Antonaras, A. The production and uses of glass in Byzantine Thessaloniki. In *New Light on Old Glass: Recent Research on Byzantine Glass and Mosaics*; James, L., Entwistle, C., Eds.; British Museum: London, UK, 2013; pp. 189–198.
9. Torp, H. *La Rotonde Palatine à Thessalonique: Architecture et Mosaïques*; Kapon Editions: Athens, Greece, 2018.
10. Bakirtzis, C.; Mastora, P.; Pitsalidis, N. The conservation of the mosaics of the Rotunda in Thessaloniki: An act of discovery. In Proceedings of the 10th Conference of the International Committee for the Conservation of Mosaics (ICCM), Palermo, Italy, 20–26 October 2008; pp. 214–224.
11. Bakirtzis, C.; Mastora, P. Are the mosaics in the Rotunda in Thessaloniki linked to its conversion into a Christian church? In Proceedings of the IX International Symposium 'Niš and Byzantium', Niš, Serbia, 3–5 June 2010; pp. 33–45.
12. Mastora, P. Interventions to Wall Mosaics During Byzantine Period. Ph.D. Thesis, Open University of Cyprus, Nicosia, Cyprus, 2017.
13. Bakirtzis, C.; Mastora, P. *Ροτόντα Θεσσαλονίκης. Το Μαυσωλείο του Μεγάλου Κωνσταντίνου, ο Ναός των Αγίων Ασωμάτων*; Υπουργείο Πολιτισμού και Αθλητισμού, ΣΗΜΑ Εκδοτική: Αθήνα, Greece, 2021.
14. Malletzidou, L.; Zorba, T.; Kyranoudi, M.; Mastora, P.; Karfaridis, D.; Vourlias, G.; Pavlidou, E.; Paraskevopoulos, K.M. The dome of Rotunda in Thessaloniki: Investigation of a multi-pictorial phase wall painting through analytical methods. *Spectrochim. Acta A Mol. Biomol. Spectrosc.* **2021**, *262*, 120116. [CrossRef]

15. Sotiropoulou, S.; Kyranoudi, M.; Raptis, K. Preliminary considerations on the technology of manufacture of glass mosaics tesserae of the Rotunda in Thessaloniki, based on in situ colour and XRF measurements. In Proceedings of the TECHNART 2017 Non-Destructive and Microanalytical Techniques in Art and Cultural Heritage, Bilbao, Spain, 2–6 May 2017.
16. Bakirtzis, C.; Kourkoutidou-Nikolaidou, E.; Mavropoulou-Tsioumi, C. *Mosaics of Thessaloniki, 4th–14th Century*; Kapon Editions: Athens, Greece, 2012.
17. Mentzos, A.; Pliota, A. *Impressions: Byzantine Thessalonike through the Photographs and Drawings of the British School at Athens (1888–1910)*; Centre for Byzantine Research: Thessaloniki, Greece, 2012.
18. Munsell Color (Firm). *Geological Rock-Color Chart: With Genuine Munsell Color Chips*; Munsell Color: Grand Rapids, MI, USA, 2011.
19. Bidegaray, A.I.; Nys, K.; Silvestri, A.; Cosyns, P.; Meulebroeck, W.; Terryn, H.; Godet, S.; Ceglia, A. 50 shades of colour: How thickness, iron redox and manganese/antimony contents influence perceived and intrinsic colour in Roman glass. *Archaeol. Anthropol. Sci.* **2020**, *12*, 109. [CrossRef]
20. Verità, M. Technology and deterioration of vitreous mosaic tesserae. *Stud. Conserv.* **2000**, *45* (Suppl. S1), 65–76. [CrossRef]
21. Neri, E.; Verità, M.; Biron, I.; Guerra, M.F. Glass and gold: Analyses of 4th–12th Levantine mosaic tesserae. A contribution to technological and chronological knowledge. *J. Archaeol. Sci.* **2016**, *70*, 158–171. [CrossRef]
22. Noboru, O.; Robertson, A. *Colorimetry: Fundamentals and Applications*; John Wiley & Sons Inc.: Hoboken, NJ, USA, 2006.
23. Mokrzycki, W.; Tatol, M. Perceptual difference in Lab* color space as the base for object colour identification. In Proceedings of the 1st International Conference on Image Processing & Communications, Bydgoszcz, Poland, 16–18 September 2009. [CrossRef]
24. Sappi Fine Paper North America. Defining and Communicating Color: The CIELAB System. Available online: https://www.sappi.com/files/cielab-technical-guide-pdf (accessed on 28 June 2023).
25. Arletti, R.; Conte, S.; Vandini, M.; Fiori, C.; Bracci, S.; Bacci, M.; Porcinai, M. Florence Baptistery: Chemical and mineralogical investigation of glass mosaic tesserae. *J. Archaeol. Sci.* **2011**, *38*, 79–88. [CrossRef]
26. Davison, S. *The Conservation and Restoration of Glass*, 2nd ed.; Butterworth-Heinemann: Oxford, UK, 2003.
27. Papadopoulos, N.; Drosou, C.A. Influence of weather conditions on glass properties. *J. Univ. Chem. Technol. Metall.* **2012**, *47*, 429–439.
28. Melcher, M.; Schreiner, M. Glass degradation by liquids and atmospheric agents. In *Modern Methods for Analysing Archaeological and Historical Glass*; Janssens, K., Ed.; Wiley: Chichester, UK, 2013; pp. 609–642.
29. Loukopoulou, P. Glass Corrosion Mechanisms and Their Restoration. Ph.D. Thesis, National Technical University of Athens, Athens, Greece, 2014.
30. Alawneh, F.; Al Shiyab, A.; Al Sekheneh, W. Chemical analysis of Late Roman glass from Quasr Al Rabbah, Jordan. *Mediterr. Archaeol. Archaeom.* **2017**, *17*, 201–213.
31. Micheletti, F.; Orsilli, J.; Melada, J.; Gargano, M.; Ludwig, N.; Bonizzoni, L. The role of IRT in the archaeometric study of ancient glass through XRF and FORS. *Microchem. J.* **2020**, *153*, 104388. [CrossRef]
32. Galli, S.; Mastelloni, M.; Ponterio, R.; Sabatino, G.; Triscari, M. Raman and scanning electron microscopy and energy dispersive X-ray techniques for the characterization of colouring and opaquening agents in Roman mosaic glass tesserae. *J. Raman Spectrosc.* **2004**, *35*, 622–627. [CrossRef]
33. Freestone, I.; Bimson, M.; Duckton, D. Compositional categories of Byzantine glass tesserae. In Proceedings of the Annales du 11e Congrès de l'Association Internationale pour l'Histoire du Verre, Bâle, Switzerland, 29 August–3 September 1988; pp. 271–280.
34. Schibille, N.; Degryse, P.; Corremans, M.; Specht, C.G. Chemical characterisation of glass mosaic tesserae from sixth-century Sagalassos (south-west Turkey): Chronology and production techniques. *J. Archaeol. Sci.* **2012**, *39*, 1480–1492. [CrossRef]
35. Boschetti, C.; Henderson, J.; Evans, J.; Leonelli, C. Mosaic tesserae from Italy and the production of Mediterranean coloured glass (4th century BCE–4th century CE). Part I: Chemical composition and technology. *J. Archaeol. Sci. Rep.* **2016**, *7*, 303–311. [CrossRef]
36. Rasmussen, K.L.; Delbey, T.; Jørgensen, B.; Jensen, K.H.; Poulsen, B.; Pedersen, P. Materials and technology of mosaics from the House of Charidemos at Halikarnassos (Bodrum, Turkey). *Herit. Sci.* **2022**, *10*, 62. [CrossRef]
37. Paynter, S. Experiments in the reconstruction of Roman wood-fired glassworking furnaces: Waste products and their formation processes. *J. Glass Stud.* **2008**, *50*, 271–290.
38. Henderson, J. *Ancient Glass, An Interdisciplinary Exploration*; Cambridge University Press: Cambridge, UK, 2013.
39. Freestone, I. Glass production in the first millennium CE: A compositional perspective. In *Ancient Glass and Glass Production*; Klimscha, F., Ed.; Berlin Studies of the Ancient World 67; Edition Topoi: Berlin, Germany, 2021; pp. 211–232. [CrossRef]
40. Wypyski, M.; Becker, L. Glassmaking technology at Antioch. In *The Arts of Antioch*; Becker, L., Kondoleon, C., Eds.; Worcester Art Museum: Worcester, MA, USA, 2005; pp. 115–175.
41. Freestone, I. The recycling and reuse of Roman glass: Analytical approaches. *J. Glass Stud.* **2015**, *57*, 29–40.
42. Jackson, C.M.; Paynter, S. A great big melting pot: Exploring patterns of glass supply, consumption and recycling in Roman Coppergate, York. *Archaeometry* **2016**, *58*, 68–95. [CrossRef]

43. Fiorentino, S.; Chinni, T.; Cirelli, E.; Arletti, R.; Conte, S.; Vandini, M. Considering the effects of the Byzantine–Islamic transition: Umayyad glass tesserae and vessels from the qasr of Khirbet al-Mafjar (Jericho, Palestine). *Archaeol. Anthropol. Sci.* **2018**, *10*, 223–245. [CrossRef]
44. Silvestri, A.; Maltoni, S.; Gianandrea, M.; Deiana, R.; Croci, C. The glass mosaic of *S. Agnese fuori le mura*: New tesserae in the puzzle of early medieval Rome. *Heritage* **2024**, *7*, 4562–4591. [CrossRef]
45. Marii, F.; Rehren, T. Archaeological coloured glass cakes and tesserae from the Petra church. In *Annales du 17e Congrès de l'Association Internationale Pour l'Histoire du Verre*; Janssens, K., Ed.; UPA: Anvers, Belgium, 2006; pp. 295–300.
46. Vandini, M.; Fiori, C.; Cametti, R. Classification and technology of Byzantine mosaic glass. *Ann. Chim.* **2006**, *96*, 587–599. [CrossRef] [PubMed]
47. Silvestri, A.; Tonietto, S.; Molin, G.; Guerriero, P. The palaeo-Christian glass mosaic of St. Prosdocimus (Padova, Italy): Archaeometric characterization of tesserae with copper- or tin-based opacifiers. *J. Archaeol. Sci.* **2014**, *42*, 51–67. [CrossRef]
48. Gliozzo, E. The composition of colourless glass: A review. *Archaeol. Anthropol. Sci* **2017**, *9*, 455–483. [CrossRef]
49. Neri, E.; Verità, M.; Conventi, A. Glass mosaic tesserae from the 5th to 6th century Baptistery of San Giovanni alle Fonti, Milan, Italy: Analytical investigations. In *New Light on Old Glass: Recent Research on Byzantine Mosaics and Glass*; James, L., Entwistle, C., Eds.; British Museum: London, UK, 2013; pp. 1–10.
50. Maltoni, S.; Silvestri, A. Innovation and tradition in the fourth century mosaic of the Casa delle Bestie Ferite in Aquileia, Italy: Archaeometric characterisation of the glass tesserae. *Archaeol. Anthropol. Sci.* **2016**, *8*, 617–633. [CrossRef]
51. Neri, E.; Jackson, M.; O'Hea, M.; Gregory, T.; Blet-Lemarquand, M.; Schibille, N. Analyses of glass tesserae from Kilise Tepe: New insights into an early Byzantine production technology. *J. Archaeol. Sci. Rep.* **2017**, *11*, 600–612. [CrossRef]
52. Maltoni, S.; Silvestri, A. Investigating a Byzantine technology: Experimental replicas of Ca-phosphate opacified glass. *J. Cult. Herit.* **2019**, *39*, 251–259. [CrossRef]
53. Bandiera, M.; Lehuédé, P.; Verità, M.; Alves, L.; Biron, I.; Vilarigues, M. Nanotechnology in Roman opaque red glass from the 2nd century AD: Archaeometric investigation in red sectilia from the decoration of the Lucius Verus Villa in Rome. *Heritage* **2019**, *2*, 2597–2611. [CrossRef]
54. Silvestri, A.; Nestola, F.; Peruzzo, L. Multi-methodological characterisation of calcium phosphate in late-antique glass mosaic tesserae. *Microchem. J.* **2016**, *126*, 462–469. [CrossRef]
55. Serra, C.L.; Silvestri, A.; Molin, G. Appendix: Archaeometric characterization. In *Lachin, M.T. Vitreous Mosaic from Tyana (Cappadocia)*; Lafli, E., Ed.; Colloquia Anatolica et Aegaea Acta Congressus Communis Omnium Gentium Smyrnae II.; Ege Yayınları: İzmir, Turkey, 2009; pp. 171–183.
56. Neri, E.; Morvan, C.; Colomban, P.; Guerra, M.F.; Prigent, V. Late Roman and Byzantine mosaic opaque "glass-ceramics" tesserae (5th–9th century). *Ceram. Int.* **2016**, *42*, 18859–18869. [CrossRef]
57. Silvestri, A.; Tonietto, S.; Molin, G.; Guerriero, P. Multi-methodological study of palaeo-Christian glass mosaic tesserae of St. Maria Mater Domini (Vicenza, Italy). *Eur. J. Mineral.* **2015**, *27*, 225–245. [CrossRef]
58. Henriques, J.M.; Barboza, C.A.; Albuquerque, E.L.; Caetano, E.W.S.; Freire, V.N.; Da Costa, J.A.P. First-principles calculations of structural, electronic and optical properties of orthorhombic $CaPbO_3$. *J. Phys. D Appl. Phys.* **2008**, *41*, 045404. [CrossRef]
59. Matin, M. Tin-based opacifiers in archaeological glass and ceramics glazes: A review and new perspectives. *Archaeol. Anthropol. Sci.* **2019**, *11*, 1155–1167. [CrossRef]
60. Tite, M.; Pradell, T.; Shortland, A.J. Discovery, production and use of tin-based opacifiers in glasses, enamels and glazes from the Late Iron Age onwards: A reassessment. *Archaeometry* **2008**, *50*, 67–84. [CrossRef]
61. Wypyski, M. Technical analysis of glass mosaic tesserae from Amorium. *Dumbart. Oaks Pap.* **2005**, *59*, 183–192. [CrossRef]
62. Van der Linden, V.; Cosyns, P.; Schalm, O.; Cagno, S.; Nys, K.; Janssens, K.; Nowak, A.; Wagner, B.; Bulska, E. Deeply coloured and black glass in the northern provinces of the Roman Empire: Differences and similarities in chemical composition before and after AD 150. *Archaeometry* **2009**, *51*, 822–844. [CrossRef]
63. Gliozzo, E.; Santagostino Barbone, A.; Turchiano, M.; Memmi, I.; Volpe, G. The coloured tesserae decorating the vaults of the Faragola Balneum (Ascoli Satriano, Foggia, Southern Italy). *Archaeometry* **2012**, *54*, 311–331. [CrossRef]
64. Maltoni, S.; Silvestri, A. A mosaic of colors: Investigating production technologies of Roman glass tesserae from northeastern Italy. *Minerals* **2018**, *8*, 255. [CrossRef]
65. Fiorentino, S. A tale of two legacies: Byzantine and Egyptian influences in the manufacture and supply of glass tesserae under the Umayyad Caliphate (661–750 AD). *Heritage* **2021**, *4*, 2810–2834. [CrossRef]
66. Di Bella, M.; Quartieri, S.; Sabatino, G.; Santalucia, F.; Triscari, M. The glass mosaics tesserae of "Villa del Casale" (Piazza Armerina, Italy): A multitechnique archaeometric study. *Archaeol. Anthropol. Sci.* **2014**, *6*, 345–362. [CrossRef]
67. Kyranoudi, M.; Malletzidou, L.; Zorba, T.; Vourlias, G.; Melfos, V.; Pavlidou, E.; Chrissafis, K. Glass mosaic tesserae from the Rotunda of Thessaloniki: Microstructural and spectroscopic characterization. *Appl. Res.* **2024**, *3*, e202300120. [CrossRef]
68. Freestone, I. Composition and microstructure of early opaque red glass. In *Early Vitreous Materials*; Shortland, A.J., Ed.; British Museum Occasional Paper 56; The British Museum: London, UK, 1987; pp. 173–191.

69. Silvestri, A.; Tonietto, S.; D'Acapito, F.; Molin, G. The role of copper on colour of the palaeo-Christian glass mosaic tesserae: An XAS study. *J. Cult. Herit.* **2012**, *13*, 137–144. [CrossRef]
70. Fiori, C. Production technology of Byzantine red mosaic glasses. *Ceram. Int.* **2015**, *41*, 3152–3157. [CrossRef]
71. Boschetti, C.; Nikita, K.; Veronesi, P.; Henderson, J.; Leonelli, C.; Andreescu-Treadgold, I. Glass in mosaic tesserae: Two interdisciplinary research projects. In *Annales du 18e Congrès de l'Association Internationale Pour l'Histoire du Verre*; Ignatiadou, D., Antonaras, A., Eds.; ASP: Thessaloniki, Greece, 2009; pp. 145–150.
72. Crocco, R.; Huisman, H.; Sablerolles, Y.; Henderson, J.; van Os, B.; Nieuwhof, A. Hunting colours: Origin and reuse of glass tesserae from the Wierum terp. *Archaeol. Anthropol. Sci.* **2021**, *13*, 155. [CrossRef]
73. Brill, R.H. *Chemical Analyses of Early Glasses, Vol. 1: The Catalogue; Vol. 2: The Tables*; The Corning Museum of Glass: Corning, NY, USA, 1999.
74. Verità, M.; Santopadre, P. Unusual glass tesserae from a third century mosaic in Rome. *J. Glass Stud.* **2015**, *57*, 287–292.
75. Barca, D.; Basso, E.; Bersani, D.; Galli, G.; Invernizzi, C.; La Russa, M.F.; Lottici, P.P.; Malagodi, M.; Ruffolo, S.A. Vitreous tesserae from the calidarium mosaics of the Villa dei Quintili, Rome: Chemical composition and production technology. *Microchem. J.* **2016**, *124*, 726–735. [CrossRef]
76. Verità, M.; Lazzarini, L.; Tesser, E.; Antonelli, F. Villa del Casale (Piazza Armerina, Sicily): Stone and glass tesserae in the baths floor mosaics. *Archaeol. Anthropol. Sci.* **2019**, *11*, 373–385. [CrossRef]
77. Vataj, E.; Hobdari, E.; Röhrs, S.; Vandenabeele, P.; Civici, N. Analytical characterization of glass tesserae from mosaics of early Christian basilicas in Albania. *Appl. Phys. A* **2017**, *123*, 76. [CrossRef]
78. Neri, E.; Biron, I.; Verità, M. New insights into Byzantine glass technology from loose mosaic tesserae from Hierapolis (Turkey): PIXE/PIGE and EPMA analyses. *Archaeol. Anthropol. Sci.* **2017**, *9*, 1523–1540. [CrossRef]
79. Neri, E.; Verità, M. Glass and metal analysis of gold leaf tesserae of 1st to 9th century mosaics: A contribution to technological and chronological knowledge. *J. Archaeol. Sci.* **2013**, *40*, 4596–4606. [CrossRef]
80. James, L. *Mosaics in the Medieval World: From Late Antiquity to the Fifteenth Century*; Cambridge University Press: Cambridge, UK, 2017.
81. Schibille, N.; Sterrett-Krause, A.; Freestone, I. Glass groups, glass supply and recycling in late Roman Carthage. *Archaeol. Anthropol. Sci.* **2016**, *8*, 697–714. [CrossRef]
82. Conventi, A.; Neri, E.; Verità, M. SEM-EDS analysis of ancient gold leaf glass mosaic tesserae: A contribution to the dating of the materials. *IOP Conf. Ser. Mater. Sci. Eng.* **2012**, *32*, 012007. [CrossRef]
83. Oddy, W.A.; La Niece, S. Byzantine gold coins and jewellery: A study of gold content. *Gold Bull.* **1986**, *19*, 19–27. [CrossRef]
84. Brems, D.; Ganio, M.; Walton, M.; Degryse, P. Mediterranean sand deposits as a raw material for glass production in antiquity. In *Annales du 18e Congrès de l'Association Internationale Pour l'Histoire du Verre*; Ignatiadou, D., Antonaras, A., Eds.; ASP: Thessaloniki, Greece, 2009; pp. 120–127.
85. Neri, E.; Gratuze, B.; Schibille, N. Dating the mosaics of the Durres amphitheatre through interdisciplinary analysis. *J. Cult. Herit.* **2017**, *28*, 27–36. [CrossRef]
86. Brill, R.H.; Whitehouse, D. The Thomas Panel. *J. Glass Stud.* **1988**, *30*, 34–50.
87. Van der Werf, I.; Mangone, A.; Giannossa, L.C.; Traini, A.; Laviano, R.; Coralini, A.; Sabbatini, L. Archaeometric investigation of Roman tesserae from Herculaneum (Italy) by the combined use of complementary micro-destructive analytical techniques. *J. Archaeol. Sci.* **2009**, *36*, 2625–2634. [CrossRef]
88. Schibille, N.; McKenzie, J. Glass tesserae from Hagios Polyeuktos, Constantinople: Their early Byzantine affiliations. In *Neighbours and Successors of Rome: Traditions of Glass Production and Use in Europe and the Middle East in the Later 1st Millennium AD*; Keller, D., Price, J., Jackson, C., Eds.; Oxbow Books: Oxford, UK, 2014; pp. 114–127.
89. Neri, E. The mosaics of Durres amphitheatre: An assessment using technical observations. *AnTard* **2017**, *25*, 353–374. [CrossRef]
90. Verità, M.; Maggetti, M.; Sagui, L.; Santopadre, P. Colors of Roman glass: An investigation of the yellow sectilia in the Gorga Collection. *J. Glass Stud.* **2013**, *55*, 21–34.
91. Vataj, E.; Civici, N.; Röhrs, S.; Dilo, T.; Hobdari, E. The study of Byzantine glass mosaic tesserae from Albania using nuclear techniques. In Proceedings of the 23rd WiN Global Annual Conference: Women in Nuclear Meet Atoms for Peace, Vienna, Austria, 24–28 August 2015.
92. Nenna, M.D. Primary glass workshops in Graeco-Roman Egypt: Preliminary report on the excavations of the site of Beni Salama, Wadi Natrun. In *Glass of the Roman World*; Bayley, J., Freestone, I., Jackson, C., Eds.; Oxbow Books: Oxford, UK, 2015; pp. 53–65.

Disclaimer/Publisher's Note: The statements, opinions and data contained in all publications are solely those of the individual author(s) and contributor(s) and not of MDPI and/or the editor(s). MDPI and/or the editor(s) disclaim responsibility for any injury to people or property resulting from any ideas, methods, instructions or products referred to in the content.